Geophys. J. Int. (2001) **144,** 656–678

Solving the dynamic rupture problem with different numerical approaches and constitutive laws

A. Bizzarri,[1,2] M. Cocco,[1] D. J. Andrews[3] and E. Boschi[1,2]

[1] *Istituto Nazionale di Geofisica e Vulcanologia, Roma, Italy*
[2] *Dipartimento di Fisica, Settore di Geofisica, Università di Bologna, Italy. E-mail: bizzarri@ibogfs.df.unibo.it*
[3] *US Geological Survey, Menlo Park, California, USA*

Accepted 2000 October 30. Received 2000 October 30; in original form 2000 March 6

SUMMARY

We study the dynamic initiation, propagation and arrest of a 2-D in-plane shear rupture by solving the elastodynamic equation by using both a boundary integral equation method and a finite difference approach. For both methods we adopt different constitutive laws: a slip-weakening (SW) law, with constant weakening rate, and rate- and state-dependent friction laws (Dieterich–Ruina). Our numerical procedures allow the use of heterogeneous distributions of constitutive parameters along the fault for both formulations. We first compare the two solution methods with an SW law, emphasizing the required stability conditions to achieve a good resolution of the cohesive zone and to avoid artificial complexity in the solutions. Our modelling results show that the two methods provide very similar time histories of dynamic source parameters. We point out that, if a careful control of resolution and stability is performed, the two methods yield identical solutions. We have also compared the rupture evolution resulting from an SW and a rate- and state-dependent friction law. This comparison shows that despite the different constitutive formulations, a similar behaviour is simulated during the rupture propagation and arrest. We also observe a crack tip bifurcation and a jump in rupture velocity (approaching the *P*-wave speed) with the Dieterich–Ruina (DR) law. The rupture arrest at a barrier (high strength zone) and the barrier-healing mechanism are also reproduced by this law. However, this constitutive formulation allows the simulation of a more general and complex variety of rupture behaviours. By assuming different heterogeneous distributions of the initial constitutive parameters, we are able to model a barrier-healing as well as a self-healing process. This result suggests that if the heterogeneity of the constitutive parameters is taken into account, the different healing mechanisms can be simulated. We also study the nucleation phase duration T_n, defined as the time necessary for the crack to reach the half-length l_c. We compare the T_n values resulting from distinct simulations calculated using different constitutive laws and different sets of constitutive parameters. Our results confirm that the DR law provides a different description of the nucleation process than the SW law adopted in this study. We emphasize that the DR law yields a complete description of the rupture process, which includes the most prominent features of SW.

Key words: crack dynamics, earthquake rupture, fault healing, friction laws, slip weakening.

1 INTRODUCTION

The dynamic problem of crack propagation and arrest has been studied in the literature by using 2-D solutions, either in-plane (Andrews 1976b; Andrews & Ben-Zion 1997) or anti-plane (Andrews 1976a; Cochard & Madariaga 1994; Madariaga & Cochard 1994 and references therein), as well as by 3-D numerical approaches (Das & Kostrov 1983; Fukuyama & Madariaga 1998; Madariaga *et al.* 1998; Olsen *et al.* 1997; Nielsen *et al.* 2000). Among the different methods proposed to solve the elastodynamic equation, the boundary integral equation and the finite difference methods are the two most widely adopted (Andrews 1973, 1985, 1994; Das & Kostrov 1983; Cochard & Madariaga 1994; Madariaga & Cochard 1994 and references therein; Andrews & Ben-Zion 1997). In the present study we investigate the dynamic propagation of a 2-D

in-plane crack by using both of these numerical approaches. In spite of the numerous applications of these procedures to investigate the dynamic features of earthquake ruptures, we believe that an accurate comparison between the two solution methods is of interest and will help in discussing the required resolution intrinsic to the dynamic problem. We emphasize that such a detailed comparison has never been made in the literature.

The solution of the dynamic problem requires the choice of the constitutive law that relates the total dynamic traction to the friction law. Different possibilities are present in the literature. Most of the applications rely on two distinct groups of constitutive relations: the slip-weakening (SW) (Andrews 1976a,b; Harris & Day 1997; Ide & Takeo 1997; Guatteri & Spudich, 2000) and the rate- and state-dependent laws (Dieterich 1986, 1992, 1994 and references therein; Ruina 1980, 1983; Gu *et al*. 1984; Perrin *et al*. 1995; Zheng & Rice 1998; Ranjith & Rice 1999). The former assumes that friction (or total traction) is a function of the fault slip only, while the latter implies that the friction is a function of slip velocity and state variables. In performing our methodological comparison we use both of these constitutive relations. This is important since most of the applications aimed at reproducing the rupture history during a single earthquake rely on the SW formalism (Andrews 1976a,b; Guatteri & Spudich, 2000).

Different rate- and state-dependent constitutive laws have been proposed (see Marone 1998 and references therein). The most common difference concerns the evolution equation adopted for the state variable (Beeler *et al*. 1994). Moreover, since the proposed laws have different singularities for a locked fault (i.e. zero slip velocity) as well as for very large slip velocities, numerous different regularizations have been suggested. These redundant analytical formulations raise the question of which is the most suitable law, or if we really need so many modifications of the constitutive law. We discuss these implications in this paper.

Another important topic for the study of the dynamic rupture evolution is the role played by heterogeneous distributions of the constitutive parameters. Several studies have investigated the effects of spatial heterogeneities of the constitutive properties (Papageorgiou & Aki 1983; Marone & Scholz 1988; Ide & Takeo 1997 and many others). Das & Aki (1977b) studied the rupture propagation with lateral variations of the strength parameter S. Evidence of spatial heterogeneity of the SW constitutive parameters also results from stick-slip experiments (Ohnaka 1996 and references therein). A heterogeneous distribution of the pre-stress on the fault plane can be caused by the stress redistribution processes from earlier seismic events (Perfettini *et al*. 1999). Rice (1993) and Boatwright & Cocco (1996) emphasized the role of the heterogeneous distribution of rate- and state-dependent constitutive parameters and the frictional control on crustal faulting episodes. In the present paper, we also use non-uniform distributions of the constitutive parameters along the fault line. This allows us to investigate the effects of the heterogeneities on the dynamic rupture propagation and arrest.

In recent years, the problem of rupture initiation has been studied either theoretically or experimentally, and there were few attempts in constraining such dynamic features by using recorded seismograms (e.g. Iio 1995; Ellsworth & Beroza 1995). Recently, Campillo & Ionescu (1997) have derived an analytical expression for the displacement arising from an anti-plane shear crack under an SW governing equation, but only in the quasi-static initiation temporal domain. No solutions in closed form exist for the intrinsically non-linear fully dynamic spontaneous problem and therefore all the solutions presented in the last five decades were obtained by means of numerical methods. In the present paper, we also discuss the different description of the initiation process resulting from the two constitutive formulations we have used to solve the dynamic crack propagation problem.

2 SOLUTION OF THE DYNAMIC PROBLEM: NUMERICAL METHODS

In this work we solve the elastodynamic equation

$$\rho \ddot{u}_i = \sigma_{ij,j} + f_i \tag{2.1}$$

for a 2-D in-plane shear crack for which the displacement and the shear traction depend on time and one spatial coordinate and we neglect the body forces ($f_i = 0$). In eq. (2.1), ρ is the mass density, u is the displacement and $\sigma_{ij,j}$ is the spatial derivative of the stress tensor. In particular, we assume that the crack propagates along x_1 in the $x_3 = 0$ plane. The medium is assumed to be infinite, homogeneous and elastic everywhere except along the fracture line. We solve eq. (2.1) by using two different methods: a boundary integral equation (BIE) method and a finite difference (FD) approach. We briefly summarize in the following the main features of our numerical solutions.

2.1 The boundary integral equation (BIE) method

In order to solve eq. (2.1) we have implemented the boundary integral equation method originally proposed by Andrews (1985). We refer to that paper for a complete description of the numerical solution. We describe here only the main features of the numerical approach. In these first applications we use an SW constitutive law for a homogeneous fault, but in the following we also consider spatially heterogeneous distributions of constitutive parameters.

Let us denote by σ_{ij}^0 the initial stress tensor and by σ_{ij}^{p} the dynamic stress perturbation due to the dynamic propagation of the crack. The integral solution of the dynamic problem in the general 3-D case is (see Kostrov & Das 1988)

$$u_n(\mathbf{x}, t) = \int_{-\infty}^{+\infty} d\tau \int_{\mathscr{S}_c(\tau)} G_{n\alpha}(\mathbf{x} - \xi, t - \tau)\sigma_{\alpha 3}^{\mathrm{p}}(\xi, \tau)\, d\Sigma_\xi ; \tag{2.2}$$

$n = 1, 2, 3;\ \alpha = 1, 2;\ \mathbf{x}, \xi \in \mathbb{R}^3$

where $\mathscr{S}_c(\tau)$ is the fractured region at the instant $t = \tau$ and $G_{n\alpha}$ is the Green tensor. Considering the problem geometry described above, assuming that for $t < 0$ the fault is in its static equilibrium $[T_1^{\mathrm{p}}(\xi_1, \tau) = 0]$ and limiting our analysis to the half-line $x_1 \geq 0$, the discretized form of (2.2) that we obtain is

$$u_1(j, m) = \sum_{k=0}^{+\infty} \sum_{n=0}^{+\infty} F_{11}(k, n) T_1^{\mathrm{p}}(j - k, m - n), \tag{2.3}$$

where the integers j and m sample the spatial and temporal coordinates, respectively, and $F_{11}(k, n)$ is the discretized Green tensor. If the spatial step Δx is greater than or equal to the product between the P-wave velocity and the time step (i.e. if $\Delta x \geq v_P \Delta t$), there is no coupling between neighbouring elements

at the time step being calculated (Andrews 1985, 1994). Therefore, it is possible to write eq. (2.3) as

$$u_1(j, m) + CT_1^{\mathrm{p}}(j, m) = \mathscr{L}_1(j, m)\,, \tag{2.4}$$

where u is the discretized slip function, T_1^{p} is the instantaneous traction at the jth point at the mth time step and C is the local compliance, or impedance, over which the instantaneous traction $T_{11}^{\mathrm{p}}(j, m)$ is averaged (Andrews 1985),

$$C \equiv -F_{11}(0, 0)\,. \tag{2.5}$$

$\mathscr{L}_1$ is a positive quantity that expresses the dynamic load resulting from the convolution of the discretized Green function $F_{11}(k, n)$ with the past (known) values of the traction T_1^{p}. The dynamic load $\mathscr{L}_1$ can be written as

$$\begin{cases} \mathscr{L}_1(j, 0) = 0\,; & \forall j \\ \mathscr{L}_1(j, m) = \displaystyle\sum_{n=1}^{m} \sum_{k=0}^{j} F_{11}(k, n) T_1^{\mathrm{p}}(j-k, m-n)\,; & m \geq 1,\ \forall j \end{cases}, \tag{2.6}$$

with $j \geq 0$. At each time step m, the total shear traction is given by the sum of the initial and the instantaneous tractions $(\tau_0 + T_1^{\mathrm{p}})$.

Following Andrews (1985), the numerical solution is found by inserting a trial traction T_1^{t} in eq. (2.4). If at a given time the total traction is lower than the frictional strength $\tau^{(\mathrm{SW})}$ (which is specified by the assumed constitutive equation), the solutions that result are $u_1(j, m) = u_1(j, m-1)$ and $T_1^{\mathrm{p}}(j, m) = T_1^{\mathrm{t}}(j, m)$. If on the other hand the total traction is greater then or equal to $\tau^{(\mathrm{SW})}$, the following system of equations is iteratively solved:

$$\begin{cases} \tau_0 + T_1^{\mathrm{p}}(j, m) = \tau^{(\mathrm{SW})}(u_1(j, m)) \\ u_1(j, m) + CT_1^{\mathrm{p}}(j, m) = \mathscr{L}_1(j, m) \end{cases}. \tag{2.7}$$

The frictional constitutive law is therefore required to complete the solution. In eq. (2.7) the frictional strength is defined at each point of the fault only as a function of slip; however, in general it can also be a function of slip velocity, normal stress and time, as well as other state variables. We discuss later the different constitutive laws that we use in this study.

2.2 The finite difference (FD) method

The FD numerical method used in this study was proposed by Andrews (1973) and has recently been used by Andrews & Ben-Zion (1997) and Ben-Zion & Andrews (1998). We have implemented in this work a numerical approach that allows us to include spatially variable constitutive parameters and to consider different constitutive laws. We solve the discretized equations derived from eq. (2.1),

$$\rho \frac{\partial}{\partial t} \dot{u}_1 = \frac{\partial}{\partial x_1} \Sigma_{11} + \frac{\partial}{\partial x_2} \Sigma_{12}\,, \tag{2.8a}$$

$$\rho \frac{\partial}{\partial t} \dot{u}_2 = \frac{\partial}{\partial x_1} \Sigma_{12} + \frac{\partial}{\partial x_2} \Sigma_{22}\,. \tag{2.8b}$$

In eq. (2.8), $\dot{u}_i$ indicates the time derivative of the slip and Σ_{ij} are the stress tensor components [the sum of an elastic contribution, σ_{ij}, and a viscous contribution, the latter being added as a perturbative term; see Andrews (1973) for further details]. In all simulations presented in this paper, we do not consider any viscous term, and therefore the total stress tensor Σ_{ij} in eq. (2.8) is simply equal to the elastic stress tensor σ_{ij}.

The x_1–x_2 plane is linear elastic everywhere except along the fault line x_1, where the constitutive equation is introduced. The fault is described by a number of split nodes coupled to each other by the constitutive relations. The solutions of eq. (2.8) are stepped through time by calculating the net force acting on every node, by updating the velocities and the displacements and by recalculating the internal force that every element exercises on its nodes.

We emphasize the different strategy adopted to discretize the elastodynamic equation (21) in the two numerical procedures here described. While in the BIE approach described in the previous section only the 'boundary' (i.e. the fault line) is discretized, in the FD method (as well as in all the so-called 'domain-type' numerical methods) the entire fault plane $x_3 = 0$ is discretized. In the latter approach a grid of nodes is introduced and each node is a vertex of an equilateral triangle; the choice of triangles, instead of other geometrical figures such as rectangles, for instance, has been made in order to increase the numerical efficiency (Petschek & Hanson 1968; Trulio 1964). All variables are defined in each node and therefore it is possible to consider the entire medium surrounding the fault line, possibly accounting for material heterogeneities.

3 THE CONSTITUTIVE EQUATIONS

The more general formulation for a constitutive law involves the definition of the maximum frictional strength on the fault plane, which is a function of several constitutive parameters,

$$\tau = f(u, \dot{u}, \sigma_{\mathrm{n}}^{\mathrm{eff}}, c_{\mathrm{e}}, \lambda_{\mathrm{c}}, T, \Psi)\,, \tag{3.1}$$

where u is the slip, $\dot{u}$ is the slip velocity, $\sigma_{\mathrm{n}}^{\mathrm{eff}}$ is the effective normal stress (which includes the effects of pore fluids), c_{e} is the chemical effect of the fluid pressure, λ_{c} is a parameter describing the geometric characteristics of the fault surface (roughness, fault gouge, etc.), T is the temperature and $\Psi \equiv (\Psi_1, \ldots, \Psi_N)$ is the state variable (Dieterich 1986 and references therein; Ruina 1980). Eq. (3.1) is usually called the governing equation.

The most important effect of the state variables Ψ is that they obey a specified temporal evolution law, which is established by a set of differential equations associated with the governing relation (3.1),

$$\frac{d}{dt} \Psi_i = g_i(u, \dot{u}, \sigma_{\mathrm{n}}^{\mathrm{eff}}, c_{\mathrm{e}}, \lambda_{\mathrm{c}}, T, \Psi)\,; \qquad i = 1, \ldots, N\,, \tag{3.2}$$

where the functions g_i also depend on the constitutive parameters previously defined. Eq. (3.2) is usually called the evolution equation. In this study we use two different and widely used constitutive relations to study the dynamics of crack propagation: an SW law (Ida 1972; Andrews 1976a,b) and a rate- and state-dependent friction law (Dieterich 1986). We discuss in the following sections the most prominent features of the constitutive laws used in this paper.

3.1 The slip-weakening law

The SW governing equation was originally proposed in numerical models by Ida (1972) and Andrews (1976a,b) and it represents an extension of the cohesive force concept introduced

by Barenblatt (1959a,b). This law has been widely used in the literature. Although its origins are theoretical, the weakening of friction with the increase of displacement has also been verified in laboratory experiments (Ohnaka & Yamashita 1989; Ohnaka 1993, 1996; Ohnaka & Shen 1999 and references therein). More recently, Ide & Takeo (1997), Bouchon *et al.* (1998) and Guatteri & Spudich (2000) have tried to retrieve SW behaviour and to estimate the constitutive parameters by inverting strong-motion waveforms recorded during large-magnitude earthquakes.

The SW law assumes that the frictional strength is a function only of the slip u and that in particular it results in

$$\tau = \begin{cases} \tau_u - (\tau_u - \tau_f)\,\dfrac{u}{d_0}\,, & u < d_0 \\ \tau_f\,, & u \geq d_0 \end{cases}. \tag{3.3}$$

The constitutive parameters used in this law are (Andrews 1976a,b) the initial shear stress, τ_0, the yield stress, τ_u, the frictional kinetic level, τ_f, and the characteristic slip, d_0. The length d_0 allows one to identify the cohesive zone, defined as the region where the fracture energy is released (see Fig. 1a). The fault strength reduction for increasing slip is physically reasonable because it accounts for the diminution of friction due to the progressive abrasion of the microscopic asperities existing on the surfaces in mutual contact.

Among the different formulations of the slip-dependent law proposed in the literature, their main difference concerns the weakening rate, that is, the rate of friction decrease as a function of slip (that is, the slope of the curves in Fig. 1). Matsu'ura *et al.* (1992) and Shibazaki & Matsu'ura (1998) used an exponential decrease of friction τ for increasing slip instead of a linear decrease (constant negative slope) as used by Andrews (1976a,b) and shown in Fig. 1(a). Campillo & Ionescu (1997) theoretically studied the initiation phase using an SW law. Their results led Ionescu & Campillo (1999) to propose that the initial slope of the SW curve controls the duration of the nucleation phase.

From these results, we emphasize that, if the SW curve has a variable slope, different frictional behaviour is expected. In particular, if the initial slope is positive, a slip-hardening phase precedes the SW behaviour (see Fig. 1b). Several other authors have used a slip-dependent law that includes an initial slip-hardening phase with an initial logarithmic increase of friction with u (Ohnaka & Yamashita 1989; Ohnaka 1993). We discuss later in this paper the implications of such an assumption.

In this study we use the simplest SW model, which implies a constant weakening rate during the dynamic process. This involves the nucleation process being imposed in our simulations. A slip-dependent constitutive law with varying weakening rate can be considered as a more heterogeneous version of the classical SW law proposed by Andrews (1976a,b).

3.2 The rate- and state-dependent friction laws

Rate- and state-dependent friction laws represent a more general form of constitutive relations than the SW law. They were proposed by Dieterich (1986) to explain stick-slip behaviour during laboratory experiments. In these laws the friction depends on the slip rate, $\dot{u}$, the state variable, Ψ, and the effective normal stress, σ_n^{eff} (Linker & Dieterich 1992). Although friction laws only dependent on the slip velocity were also introduced (Carlson & Langer 1989; Cochard & Madariaga 1994), we will not use these constitutive relations in this study.

We use the rate- and state-dependent constitutive relations in the following forms assuming that the normal stress, σ_n^{eff}, is constant:

$$\tau = \mu(\dot{u}, \Psi)\sigma_n^{\text{eff}}\,, \tag{3.4a}$$

$$\frac{d}{dt}\Psi = g(\dot{u}, \Psi)\sigma_n^{\text{eff}}\,, \tag{3.4b}$$

where μ is the friction coefficient and only one state variable Ψ is adopted. Both μ and g expressly dependent on the slip velocity and the state variable.

Depending on the functional form for μ and g, we have either a Dieterich–Ruina (DR) or a Ruina–Dieterich (RD) frictional constitutive relation (see Perrin *et al.* 1995; Roy & Marone 1996). These two laws differ mainly in the formulation of the evolution equation (3.4b) and consequently for the different definitions of state variables. In this paper we use only the DR law (Dieterich 1986 and references therein) in its 'original' formulation, which is described by the following equations:

$$\tau = \left[\mu_* - a\ln\left(\frac{v_*}{v} + 1\right) + b\ln\left(\frac{\Phi v_*}{L} + 1\right)\right]\sigma_n^{\text{eff}}\,, \tag{3.5a}$$

$$\frac{d}{dt}\Phi = 1 - \frac{\Phi v}{L}\,, \tag{3.5b}$$

where μ_* and v_* are arbitrary reference values of the friction coefficient and of the slip velocity, respectively, a, b and L are the constitutive parameters and Φ is the state variable. In the

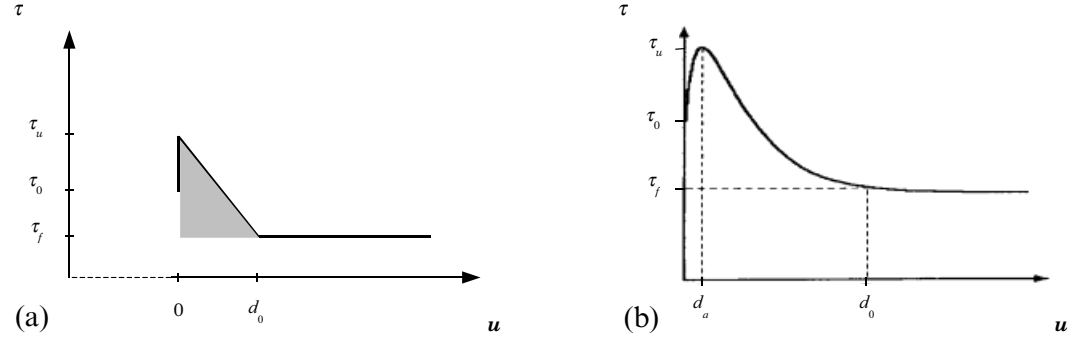

Figure 1. The SW model. (a) Constitutive law introduced by Andrews (1976a,b). When the fault starts to slip, the friction degrades from the maximum static level $\tau_u = \mu_d \sigma_n^{\text{eff}}$ to a residual frictional level $\tau_f = \mu_f \sigma_n^{\text{eff}}$ over a characteristic length d_0. σ_n^{eff} is the effective normal stress and μ is the coefficient of friction. (b) SW law proposed by Ohnaka & Yamashita (1989). The strength initially increases (slip-hardening behaviour) up to the maximum level, and later exponentially decreases to a sliding level τ_f.

DR model the state variable has the physical meaning of an average contact time between the sliding surfaces (Dieterich 1986; Ruina 1983). The evolution equation (3.5b) is usually called the slowness (or ageing) law (Ruina 1983; Beeler *et al.* 1994; Roy & Marone 1996), and it includes true ageing.

In the low-velocity limit, the state variable Φ in the DR formulation (3.5b) evolves as a linear increase in time, yielding a restrengthening process. Eq. (3.5) shows a singularity in friction when v is close to zero. For this reason several different regularized formulations have been proposed (Perrin *et al.* 1995; Zheng & Rice 1998) that use a cut-off velocity v_l (v is replaced by $v+v_l$).

The constitutive parameter $A=a\sigma_n^{\rm eff}$ represents an instantaneous rate sensitivity, that is, the direct effect of the friction after a sudden change in slip velocity. $B=b\sigma_n^{\rm eff}$ controls instead the evolution of the state variable. The characteristic distance L is the length over which the surface slips before the motion approximates steady-state sliding (Ruina 1983; Tse & Rice 1986; Rice & Tse 1986; Dieterich 1992, 1994; Perrin *et al.* 1995 and many others).

The quantity $B-A$ plays a very important role in the sliding process because it determines the sign of $(d/dv)\tau^{\rm ss}(v)$, that is, of the frictional rate under stationary conditions. Stability analyses (e.g. Rice & Ruina 1983; Gu *et al.* 1984) have pointed out that for $(d/dv)\tau^{\rm ss}>0$ (i.e. for $B-A<0$) the sliding is stable, while for $(d/dv)\tau^{\rm ss}<0$ (i.e. for $B-A>0$) the sliding is unstable. The first behaviour (aseismic) is defined in the literature as velocity strengthening, while the second (potentially seismic) is defined as velocity weakening.

4 COMPARISON BETWEEN THE NUMERICAL APPROACHES

4.1 BIE versus FD: homogeneous fault

In order to compare the two numerical approaches proposed here (BIE and FD), we have chosen to use an SW law with homogeneous constitutive parameters along the whole fracture line. We discuss in the next section further simulations with a heterogeneous distribution of constitutive parameters. The adopted SW parameters are the same for both methods. We consider a Poissonian medium, in which the elastic parameters (adimensional units) are the density $\rho=1$, the Lamé moduli $\lambda=\mu=1$, the S-wave velocity $v_S=1$ and the P-wave velocity $v_P=1.732$. In performing our simulations we often use the adimensional quantity S (Das & Aki 1977a,b),

$$S \underset{\rm df}{=} \frac{\tau_{\rm u}-\tau_0}{\tau_0-\tau_{\rm f}},$$

which is the ratio between the rise of the stress necessary to start the sliding and the dynamic stress drop.

We first discuss a numerical simulation that qualitatively reproduces the modelling results obtained by Andrews (1985) using a BIE method. We use for both adopted methods equivalent values for the SW constitutive parameters with the same spatial sampling. The rupture initiation is imposed in both approaches and the adopted numerical procedure is strictly the same: we initially impose a time-weakening in the following form:

$$\tau^{\rm (TW)}=\tau_{\rm u}-(\tau_{\rm u}-\tau_{\rm f})\,\frac{t_n-\dfrac{x_i}{v_{\rm force}}}{T_{\rm width}},$$

where $T_{\rm width}$ is equal to 0.266. In this way the crack is initially non-spontaneous, with a rupture velocity that is a fraction of the Rayleigh wave speed, $v_{\rm R}$ ($v_{\rm force}=0.7v_{\rm R}$). When the friction predicted by the imposed time-weakening becomes greater than the friction predicted by the SW law, the crack grows spontaneously. The time-weakening duration is not constant, but depends on the adopted parameters; for the simulations shown in Fig. 2 it is equal to $7\Delta t$. This figure shows the comparison between slip, slip velocity and total traction obtained by the BIE and FD methods by using 129×160 and 257×198 gridpoints in the x_1–t plane, respectively. The difference between the number of gridpoints along x_1 is due to the fact that the BIE calculation is performed in the half-line $x_1\geq0$ only. The difference of the temporal gridpoints t is due to the different value of the Courant–Friedrichs–Lewy (CFL) ratio $w=v_S\Delta t/\Delta x$, which controls the convergence of the numerical algorithms (see e.g. Fukuyama & Madariaga 1998). Our stability tests have shown that the best choice is $w^{\rm (BIE)}=v_S/v_P=0.578$ and $w^{\rm (FD)}=(0.975\ \sqrt{3}/2)\ (v_S/v_P)=0.475$.

The modelling results shown in Fig. 2 emphasize that the two numerical methods provide similar solutions; we note a crack tip bifurcation that occurs slightly earlier for the FD method. The BIE solution is identical to that obtained by Andrews (1985). After initiation, the rupture front propagates at the Rayleigh velocity, $v_{\rm R}$, while the secondary front jumps to a supershear rupture velocity and asymptotically tends to the P-wave speed, v_P. We recall that only for anti-plane 2-D cracks is the limiting velocity v_S. The time step at which the crack tip splits depends on the characteristic weakening distance, d_0; for the same S-values, the higher the value of d_0, the later the tip splitting occurs. The two approaches yield a similar slip velocity and total traction at the crack tip.

The cohesive (or breakdown) zone is shown in Figs 2(a and d) as hatched areas; these are the fault regions where the fracture energy is released and the traction decreases from the value $\tau_{\rm u}$ to the frictional level $\tau_{\rm f}$. This is expected for an SW constitutive law (Andrews 1976a,b; Ohnaka 1993). The main difference between the two solutions concerns the bifurcation, which occurs earlier in the FD case than in the BIE case. We point out that in both simulations the cohesive zone width decreases as the crack propagates far from the nucleation patch: this is due to the increase of the dynamic load caused by the larger number of points in the region that has already slipped (see eq. 2.6). The shear stress falls to a final level $\tau_{\rm f}$ over a smaller distance and during a smaller time (breakdown zone duration), although the weakening rate (determined by the stress versus the slip) remains the same. This means that the slip velocity is increasing as the crack propagates far from the nucleation zone. The analytical relation between slip velocity and breakdown duration is derived in Appendix A, where we show that, in order to have a constant d_0 (as prescribed for a homogeneous SW), the slip velocity has to increase for decreasing duration of the breakdown process. Fig. 2(g) shows the difference between the two slip functions resulting from the BIE and FD methods in the x_1–t plane by introducing a misfit function defined in Appendix B. This figure shows that the two methods provide nearly identical slip values. The main differences occur inside the breakdown zone and at the crack tip bifurcation.

Figs 3 and 4 depict the time histories of slip, slip velocity and traction (shown in Fig. 2) computed at two gridpoints ($x_1=3.9$ and 5.3). For these calculations we have increased the spatial resolution (twice for the BIE and four times for the FD

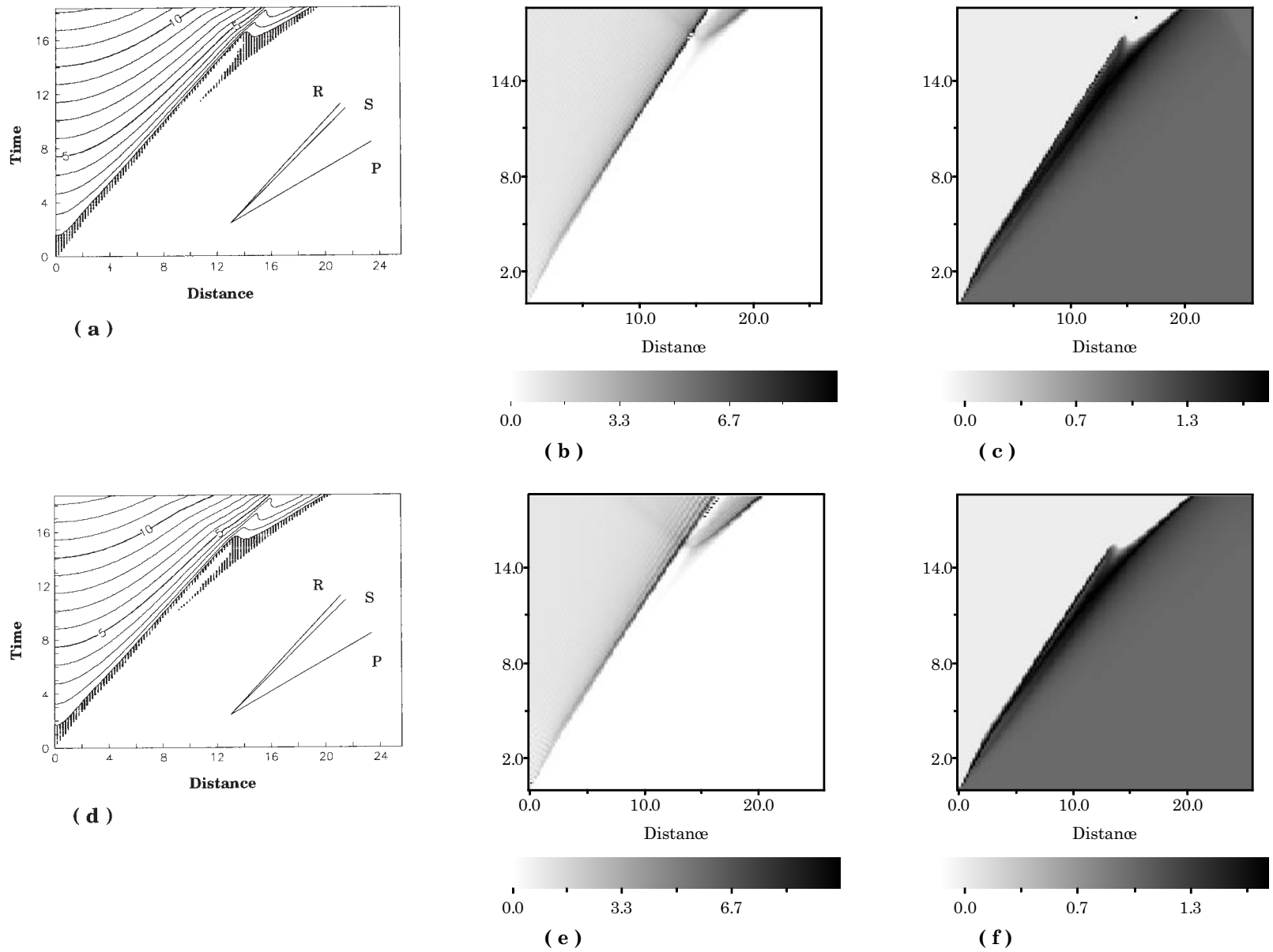

Figure 2. Numerical solutions obtained from the BIE (top) and the FD (bottom) methods for a reference case, in which the strength S is uniform on the fault ($S=0.8$). This is obtained by setting (in adimensional units) $\tau_0=1$, $\tau_u=1.8$ and $\tau_f=0$ in the BIE case and $\mu_0=1$, $\mu_u=1.8$, $\mu_f=0$ and $\sigma_n^{eff}=1$ in the FD case. In both methods we fix $d_0=1.309$ and $\Delta x=0.2$ (in adimensional units). (a) and (d) show the spatio-temporal evolution of the slip normalized by the characteristic distance d_0; the hatched area represents the fault region where the fracture energy is released. (b) and (e) show the slip velocity, while (c) and (f) show the total shear traction τ. The misfit m (Appendix B) between the slip obtained using the BIE and the FD methods is shown in (g). The straight lines in (a) and (d) represent the Rayleigh, S- and P-wave speeds. See text for details of the elastic properties of the medium surrounding the fault line.

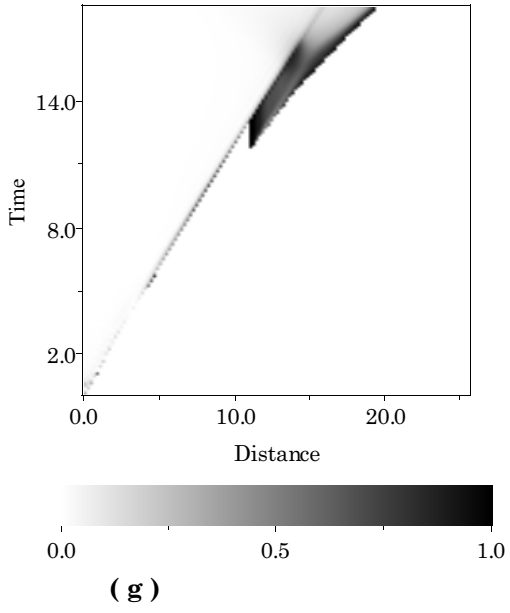

Figure 2. (*Continued.*)

method). The BIE and FD methods yield very similar time behaviours of source parameters. In particular, we note that the two methods provide similar time evolutions of the total traction and the same peak values of slip velocity.

In Figs 3(d) and 4(d) we show phase diagrams, that is, the slip rate versus the shear traction, which exhibit characteristics analogous to those experimentally obtained by Ohnaka & Yamashita (1989). When the total traction reaches the yield stress value (τ_u), the accelerating phase begins (see Figs 3d and 4d). This phase can be subdivided into an initial stage, where the traction is nearly constant for both the BIE and the FD solutions, and a subsequent sharp reduction of total traction (analytically defined as $d\tau/dt<0$ and $dv/dt>0$). The accelerating phase resulting from the two numerical approaches is slightly different. Although the rate of traction decrease resulting from the two methods is almost the same, the FD provides slightly more complex behaviour when the slip velocity reaches its maximum. We observe different behaviour between the two solutions when the slip velocity is close to its maximum value and total traction is nearly at the kinetic stress level (see the shaded boxes in Figs 3d and 4d). The FD solution always shows a fast reduction in total traction occurring at the peak slip velocity. In other words, the final drop of total traction occurs when the slip velocity is already at the maximum value. On the contrary, the BIE solution shows that the peak slip velocity is reached at the kinetic stress level (note the different shape of the phase diagram inside the shaded box). This effect is even more evident after the crack bifurcation when the rupture velocity is higher. Looking at Figs 3 and 4 it is observed that the final slip velocity is non-zero, that is, the crack is not arrested, but it continues to enlarge in time.

Our comparison indicates that if the medium is homogeneous and if the solutions have a good resolution (see Appendix C and the discussion below), the two methods provide similar results and the general behaviours of slip, slip velocity and traction are quite similar, in particular before crack bifurcation (as is seen from Fig. 2g). The phase diagrams shown in Figs 3(d) and 4(d) show that for a given slip velocity value there exist two values of dynamic traction; such an observation is consistent with the stick-slip experiments of Ohnaka & Yamashita (1989). This implies that a pure velocity-weakening constitutive law is not supported by experimental observations. This is one of the motivations for introducing the state variable (Dieterich 1986 and references therein; Ruina 1980, 1983).

Fig. 5 shows the total traction as a function of slip for the same gridpoints as used in Figs 3 and 4 for the BIE and FD solutions: both methods correctly reproduce the trend required by the SW law. We point out that the spatio–temporal sampling of our solutions provides a good resolution of the cohesive zone, as indicated by the large number of points appearing along such a line. In Appendix C we discuss the conditions that have to be satisfied in order to have the required resolution and stability of the numerical solutions. We note that these conditions have to be carefully verified since realistic spatio–temporal slip patterns can also be associated with unstable solutions. This is particularly true when complex dynamic processes are investigated, such as those resulting from heterogeneous distributions of constitutive parameters.

In order to provide further information from our methodological comparison, we also compare the CPU time and the RAM requirements to run the numerical tests discussed here. We perform these simulations with two different 256 Mbyte RAM processors: a Compaq Alpha Server 1000 A at 433 MHz and an Intel Pentium III-based Personal Workstation at 450 MHz. In each hardware configuration, the BIE code is faster with respect to the FD one, approximately by a factor of 1.5. This is due to different factors: the most important is that while the BIE code calculates the solutions of the dynamic problem only in the half-space $x_1\geq 0$, the FD code computes the solutions over the entire fault line x_1. Moreover, while in the BIE code only five real single precision arrays are necessary during the entire calculation (and therefore stored in memory), in the FD code 23 single precision arrays are stored. These include the stresses Σ_{ij} and the two components of slip velocity in the $x_3=0$ plane, outside the fault line. Such a difference implies not only a larger calculation time, but also larger RAM requirements.

4.2 BIE versus FD: heterogeneous distribution of SW parameters

Both the BIE and the FD numerical procedures used in this study have been implemented to use spatial heterogeneous distributions of the constitutive parameters for an SW law (τ_0, τ_u, τ_f and d_0). The use of a homogeneous distribution of constitutive parameters implies a constant fracture energy G that does not allow one to model the spontaneous rupture growth completely (Andrews 1985). In this section we compare the two methods by discussing the results of several simulations of a crack propagation obeying an SW law for a line source with a spatially variable distribution of dynamic parameters.

The first heterogeneous model consists of a barrier (low pre-stress and high yield stress on a finite extended patch) located in the middle of the fault (see Fig. 6). τ_0 and τ_u are equal to 1 and 1.8 everywhere except in the region $13\leq x_1\leq 17.2$, where they are 0.1 and 11, respectively. The kinetic level τ_f and the characteristic length d_0 are uniform and fixed at 0 and 2.094, respectively. In Fig. 6 we show the spatio–temporal evolution of the slip velocity obtained by the two numerical approaches. The abrupt arrest of crack propagation is evident when the

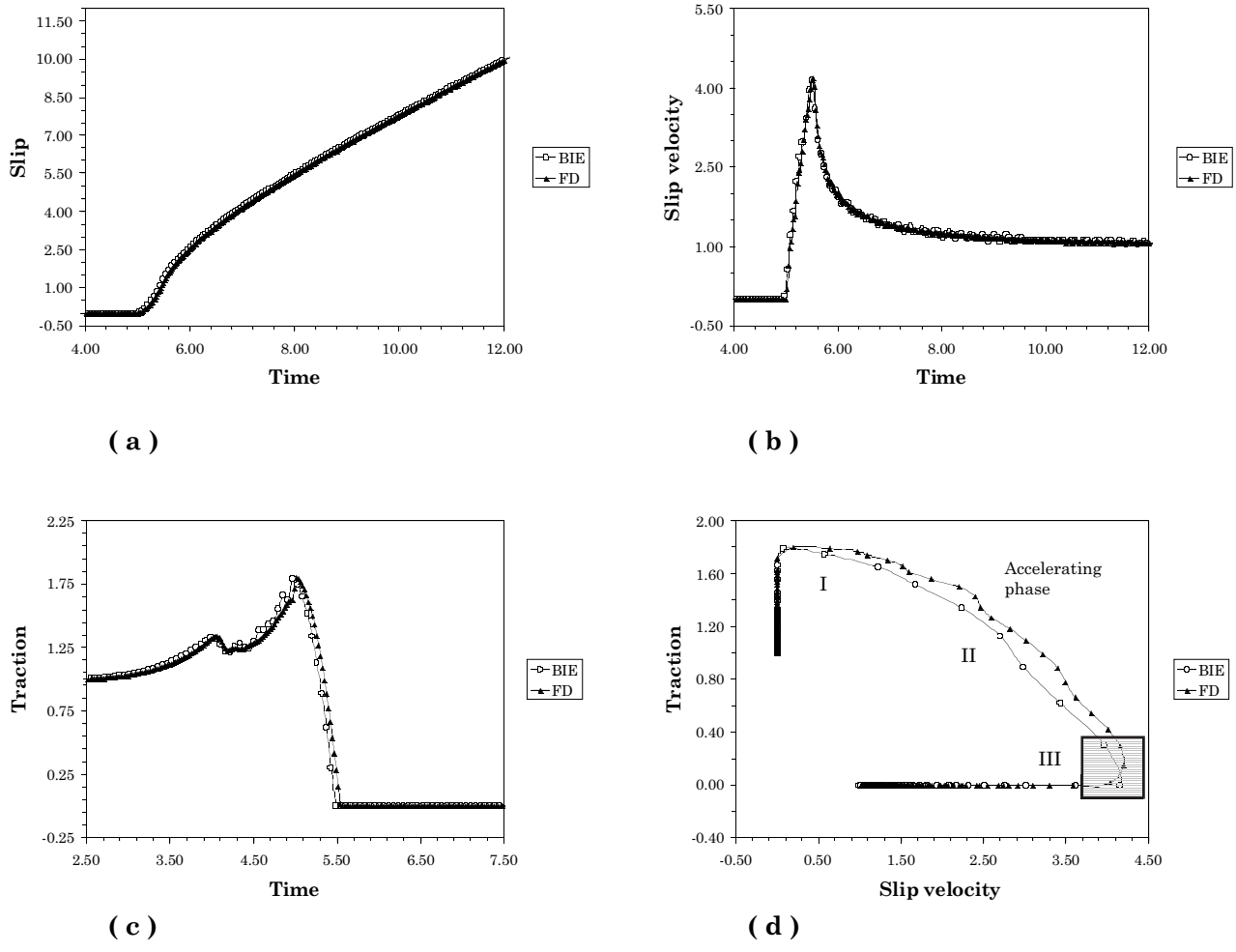

Figure 3. Time histories of (a) the slip, (b) the slip velocity, (c) the total shear traction, and (d) the phase diagram (slip rate versus traction) obtained from both numerical methods at the fault point $x_1 = 3.9$ for the simulation described in Fig. 2. I indicates the initial stage where the traction is nearly constant; II represents the sharp reduction in τ ($d\tau/dt < 0$) during which the slip velocity increases; III indicates the traction behaviour at the peak slip velocity (inside the shaded box). The shaded box indicates the different behaviour at the maximum slip velocity: while for the BIE method the maximum peak velocity is reached exactly when $\tau = \tau_f$, for the FD method there is a final drop in traction when the slip velocity is nearly at its maximum value.

rupture front reaches the barrier caused by a very high strength value (in these simulations we chose $S = 109$) in this region. This simulation allows us to model the rupture arrest. The two methods provide similar results, although the FD result is more noisy. Both solutions show a healing front back-propagating from the barrier. The slip is arrested at the barrier edge, and the slip duration is a function of the back-propagating healing front, as previously found in many other studies (Day 1982; Das & Kostrov 1983). Hereinafter we refer to this behaviour as barrier healing. Although both methods provide similar results, we note that the BIE solution is more stable.

In a second simulation we have modelled the rupture propagation on a line source with a heterogeneous distribution of the frictional stress (τ_f), as shown at the bottom of Fig. 7. The kinetic stress is 3 everywhere except in the section $5.6 \leq x_1 \leq 12.2$, where it is zero. The initial shear stress, τ_u and d_0 are 4, 4.8 and 1.309, respectively, everywhere along the entire fault line. Fig. 7 shows the results of this simulation obtained with the two methods. We observe a sharp increase of rupture velocity (crack tip speed) when the crack enters the region with low strength (S): the crack speed jumps suddenly to the P-wave velocity in both solutions. The spatio–temporal behaviour of the slip of these solutions (Figs 7a and b) is quite similar and shows the same general features as discussed above. No bifurcation exists in this configuration: the cohesive zone is resolved in a similar way by both methods. The behaviour of the total traction is also very similar for both the BIE case and the FD case (see Figs 7c and d).

5 COMPARISON BETWEEN DIFFERENT CONSTITUTIVE LAWS

In this section we present the results of several simulations calculated using the same numerical approach (the FD method) but with different constitutive laws. The choice of the FD approach is justified by the results of the comparison with the BIE solutions presented above. In these simulations we use the SW as well as the rate- and state-dependent friction laws described in Sections 3.1 and 3.2. In order to perform such a comparison it is necessary to associate the physical parameters of the different constitutive laws properly (see also Mikumo 1992). We briefly explain this in the next section.

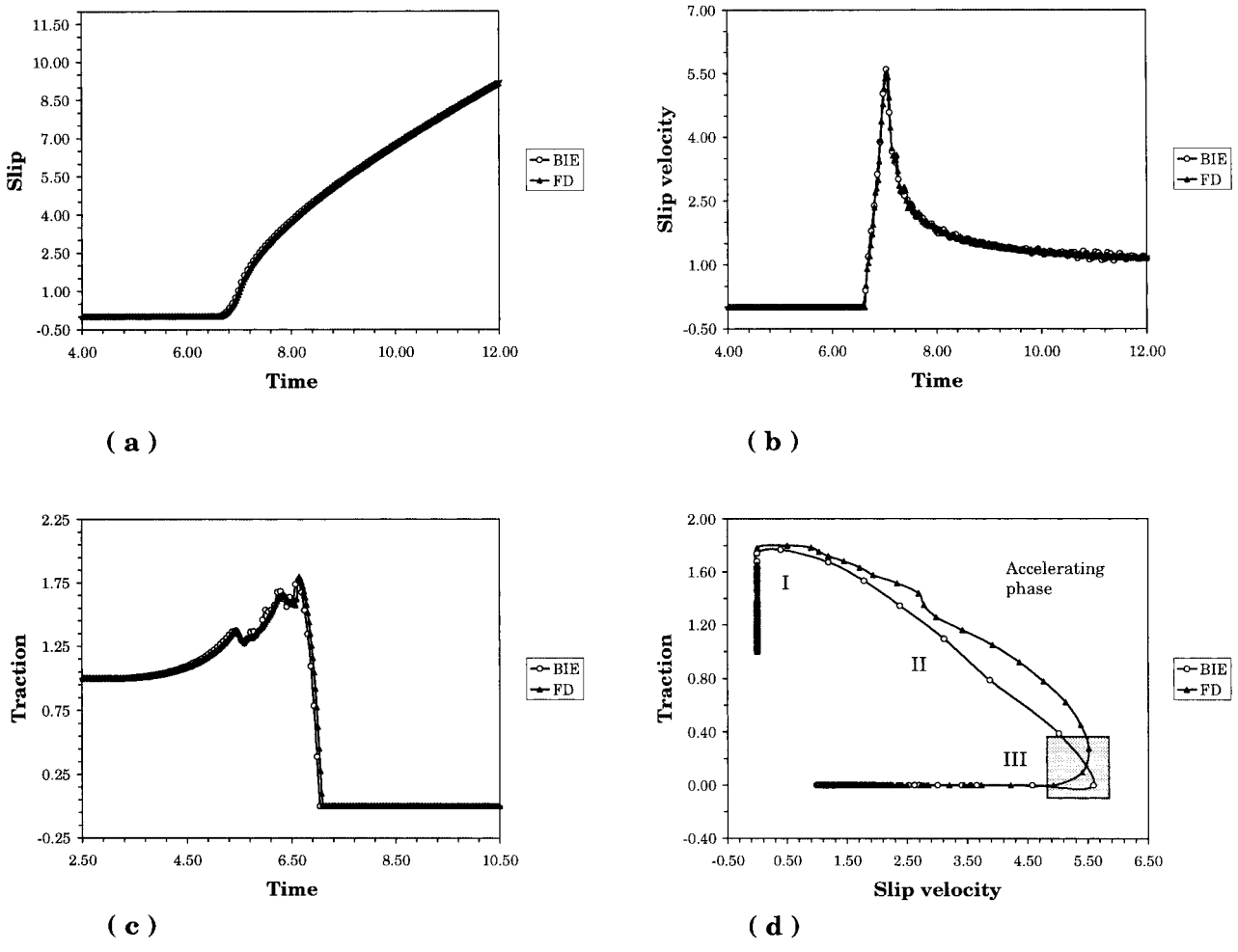

Figure 4. Same as Fig. 3 but at the fault point $x_1 = 5.3$.

5.1 Theoretical comparison between constitutive parameters

All the governing equations previously described have a characteristic length d_0 or L, intrinsic to the dynamic problem. We derive the correspondence between the different constitutive parameters (d_0 and L, τ_u and τ_f with a and b) using the results of laboratory experiments (Gu *et al.* 1984) for the response to an abrupt change in slip velocity (see Fig. 8). From a physical point of view, the yield stress in the SW model, τ_u, corresponds to the peak value of friction obtained when the slip velocity changes from an initial velocity, v_{init}, to the value v_2 (usually called the direct effect). Moreover, the kinetic friction level τ_f in the SW law corresponds to the steady-state friction $\tau^{ss}(v_2)$ in rate- and state-dependent friction laws. We propose the following associations:

$$\tau_u \leftrightarrow \tau^{ss}(v_{init}) + a\sigma_n \ln(v_2/v_{init}), \tag{5.1a}$$

$$\tau_f \leftrightarrow \tau^{ss}(v_2), \tag{5.1b}$$

where $\tau^{ss}(v)$ represents the steady-state friction. Rice (1993) described the exponential decrease of friction observed in modelling the response of a spring-slider to a velocity change (shown in Fig. 8) as

$$\tau = \tau^{ss}(v_2) + e^{-u/L}\left[\tau^{ss}(v_{init}) + a\sigma_n^{eff} \ln\left(\frac{v_2}{v_{init}}\right) - \tau^{ss}(v_2)\right].$$

This relation has been introduced to describe several common features of material response to a change in sliding velocity resulting from laboratory experiments; it has not been derived from theoretical constitutive laws. The most important feature arising from this relation is the dependence of friction on the ratio between the slip velocities. If we develop this expression, limiting it to first order for $u \ll L$, we obtain

$$\tau \cong \tau^{ss}(v_{init}) + a\sigma_n^{eff} \ln\left(\frac{v_2}{v_{init}}\right) - \left[\tau^{ss}(v_{init}) + a\sigma_n^{eff} \ln\left(\frac{v_2}{v_{init}}\right) - \tau^{ss}(v_2)\right]\frac{u}{L}.$$

Taking into account relations (5.1a) and (5.1b), this expression becomes equivalent to eq. (3.3) for the SW law when the following association is valid:

$$d_0 \leftrightarrow L. \tag{5.1c}$$

Such an analogy seems to be physically reasonable because in rate- and state-dependent laws, L represents the length over which the friction decreases to the stationary level (Ruina 1983; Dieterich 1992, 1994; Perrin *et al.* 1995). In Appendix D we also discuss the comparison concerning the fracture energy G resulting from the SW and the rate- and state-dependent friction laws. We only remark here that both constitutive formulations yield a fracture energy proportional to the characteristic length

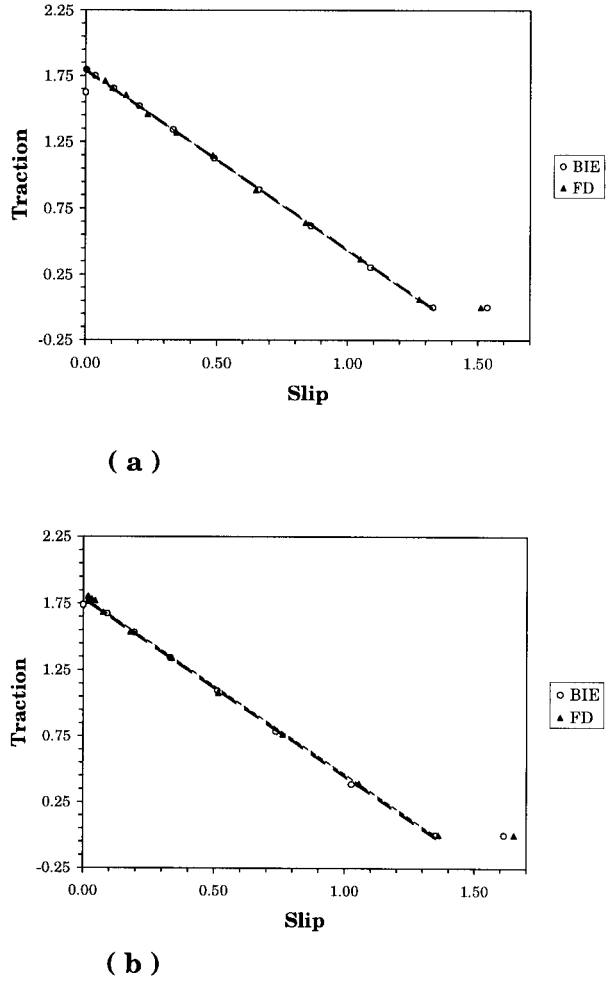

Figure 5. Traction as a function of slip resulting from the two numerical methods. (a) shows the solution for the gridpoint $x_1 = 3.9$ (same as Fig. 3); (b) shows the solution for $x_1 = 5.3$ (same as Fig. 4). The dashed lines represent a linear regression and identify the constant weakening rate. This figure was drawn by fixing the same time steps for the two methods.

and the difference between the yield stress (eq. 5.1a) and the kinetic friction level (eq. 5.1b). This implies that for both constitutive laws there exists a critical patch size, that is, a minimum dimension for which a crack can propagate. In Appendix C we discuss the definitions of the critical patch size.

5.2 Dieterich–Ruina laws versus slip-weakening

In this section we use the FD method with different constitutive equations: we use both the SW and the DR laws. In order to account for the continuous variations of u, Φ and τ, the solution resulting from rate- and state-dependent constitutive laws requires a substepping in time, which is resolved by using a Rosenbrock stiff integration procedure (Press *et al.* 1992), preferred to the Runge–Kutta method for reasons of numerical efficiency.

We model a velocity weakening behaviour where the parameters a and b are uniform on the fault line (equal to 0.75 and 1.6, respectively; see Table 1). According to Boatwright & Cocco (1996), this configuration corresponds to a very velocity-weakening field ($B - A \gg 0$); in the following we will refer to this field as a strong seismic regime. The adopted set of initial parameters at $t = 0$ along the whole fault line is listed in Table 1; the shear traction is always in the steady state at $t = 0$, while the state variable is in the steady state except in the nucleation region ($10\Delta x$ wide). In Figs 9(a)–(c) we show the results of this simulation, which is characterized by a large stress drop and considerable slip.

Table 1. Input parameters, in non-dimensional units, used in the simulations. The reference coefficient of friction μ^* is assumed to be 0 for simplicity and we chose $\Delta x = 0.1$ in the SW simulations.

Dieterich–Ruina law	Slip-weakening law
$\mu^* = 0$	
$\sigma_n^{eff} = 1$	
$a = 0.75$	$\tau_u = 18.60196$
$b = 1.6$	$\tau_f = 12.32062$
$L = 1.6$	$d_0 = 1.6$
$v_{init} = 9 \times 10^{-2}$	
$\Phi(x_1, t = 0) = \begin{cases} \Phi_{nucl} = 4 \times 10^{-3}, & x_1 \in [-1, 1] \\ \Phi^{ss}(v_{init}), & \text{elsewhere} \end{cases}$	
$\tau_0 \equiv \tau(x_1, t = 0) = \tau^{ss}[v_{init}] = 15.65758$	$\tau_0 = 15.65758$
$\Delta x = 0.2$	$\Delta x = 0.1$

The simulation for an SW constitutive law is obtained by using the proper constitutive parameters resulting from the relations (5.1) previously derived. In particular, we have used $\tau_0 = \tau^{ss}(v_{init})$; v_2 is obtained from the state variable. We first run the FD code using the rate- and state-dependent constitutive law. As described in the following, we verify that after the stress release the state variable is in the steady state, that is, $\Phi^{ss}(v_2) = L/v_2$. Therefore, since we know Φ and L, we are able to derive the proper value of v_2. From eq. (5.1) we have consequently determined the SW parameters τ_u and τ_f. Finally, we have chosen the same characteristic length for the two constitutive relations: $d_0 = L$. The resulting values are listed in Table 1 and they yield a strength parameter S equal to 0.88. The solutions obtained using the SW constitutive law are shown in Figs 9(d)–(f).

The comparison between these solutions also shows that with the rate- and state-dependent friction laws it is possible to model a highly unstable regime in which the dynamic load produces a bifurcation of the rupture front with a crack tip propagation velocity approaching v_P. Nevertheless, in the SW solution (Figs 9d–f) the tip splitting occurs much earlier than in the DR solution. This is due to the different behaviours of the constitutive laws during the nucleation phase. We note that our SW law has a constant weakening rate. On the other hand, the rate- and state-dependent friction law has an initial evolution that is quasi-static, with very low slip velocities (compare Figs 9b and e). This effect is evident in the 3-D views of the shear traction (Figs 9c and f): with the DR law the stress gradually increases to reach the maximum value and then decreases as far as the final level, whereas with the SW law the dynamic process is more immediate. This feature is intrinsic to our SW law even when very low initial velocities (v_{init}) are used. As a consequence, the rupture acceleration is much faster for the SW law than for the DR law; worthy of note is the gradual variation of rupture velocity in Figs 9(a) and (b). In order to show this feature, we have plotted in Fig. 10 the crack tip

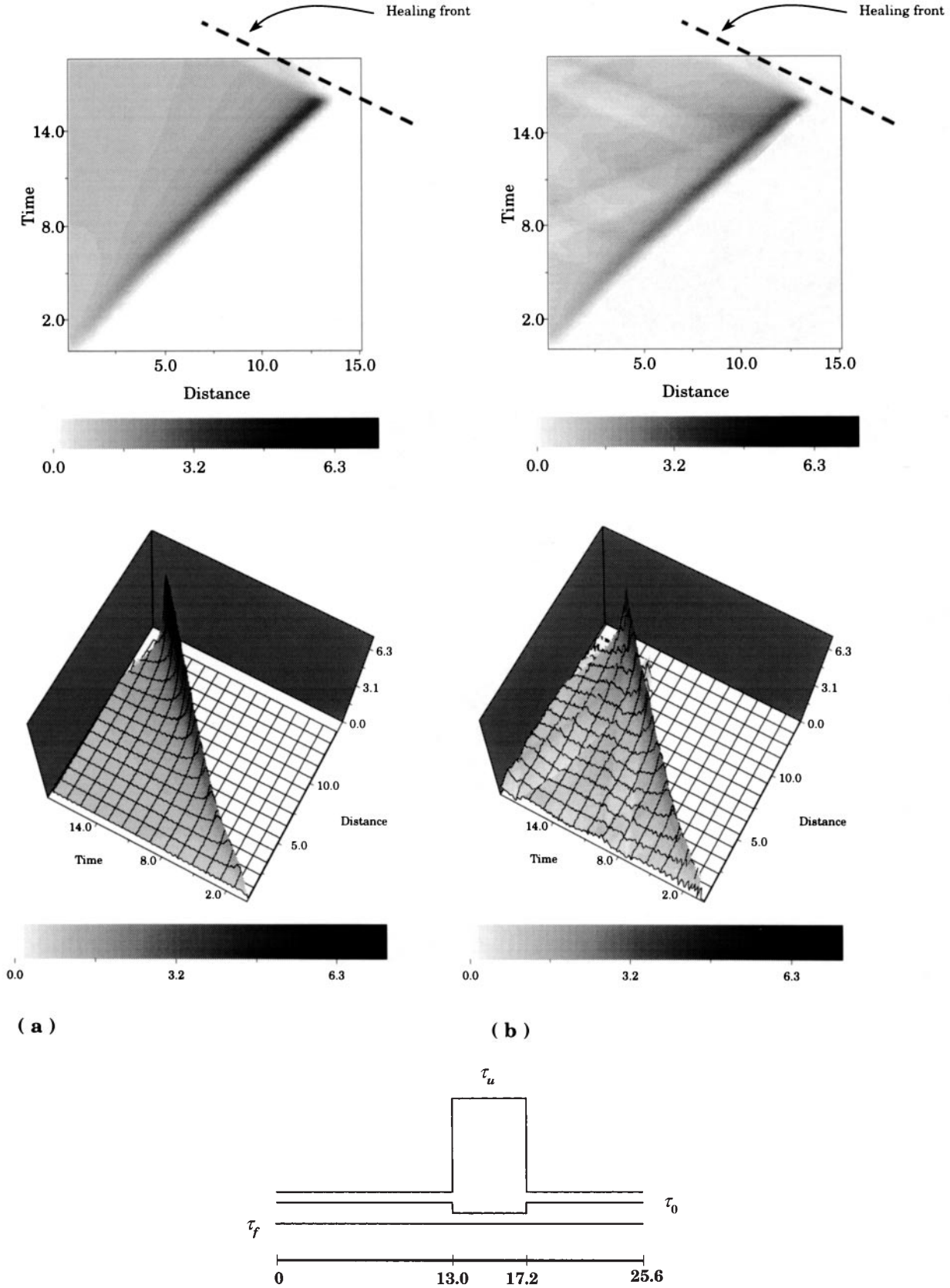

Figure 6. Slip velocity behaviour for a heterogeneous strength model, which reproduces a barrier-healing phase. In both (a) the BIE and (b) the FD cases, $\tau_0 = 1$ and $\tau_u = 1.8$ everywhere except in the area $13 \leq x_1 \leq 17.2$, where $\tau_0 = 0.1$ and $\tau_u = 11$. The parameters τ_f and d_0 are uniform and are 0 and 2.094, respectively. The solutions are plotted in a portion of the entire fault length in order to emphasize the arrest process. The distribution of constitutive parameters along the fault line is depicted in the sketch at the bottom. The dashed lines in the top panels indicate the back-propagating healing front.

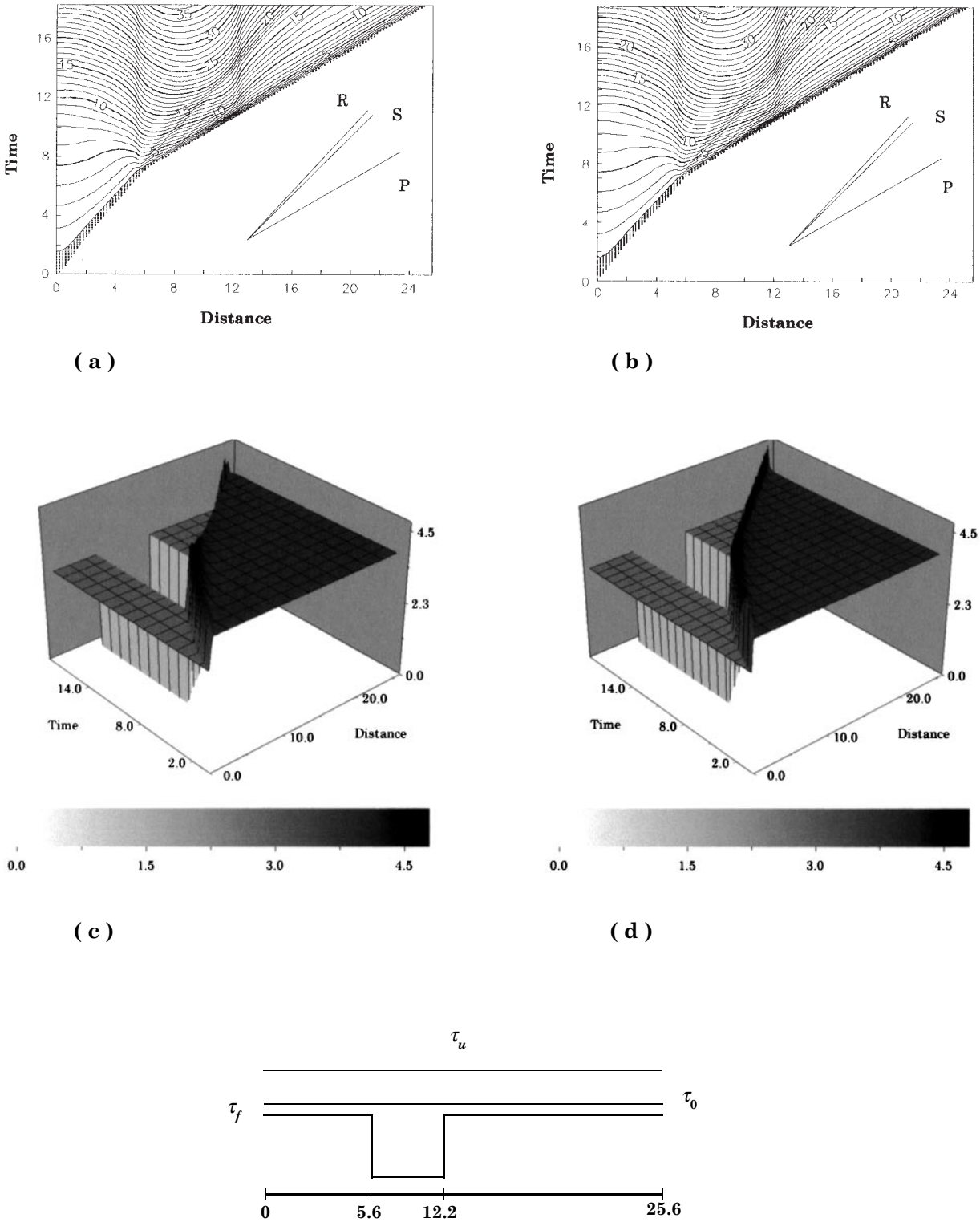

Figure 7. Normalized slip obtained for a configuration in which only τ_f is heterogeneous. $\tau_f = 3$ everywhere, except in $5.6 \leq x_1 \leq 12$, where it is 0. Other parameters are $\tau_0 = 4$, $\tau_u = 4.8$ and $d_0 = 1.309$. (a) and (b) show the slip and (c) and (d) show a 3-D view of traction for the BIE and FD cases, respectively. The geometry of the spatial distribution of the frictional parameters is shown in the sketch.

velocity as a function of time. This figure shows that the crack tip acceleration is higher for the SW solution than for the DR solution, even if both methods provide a similar range of variability for the rupture velocity. Moreover, the initial velocity of the DR model is lower than that of the SW solution. Although under less general physical conditions, the crack tip bifurcation obtained with the DR law was obtained by Okubo (1989) using a BIE numerical approach.

The basic assumption we made in using equivalent constitutive parameters in both friction laws is that after the stress drop the

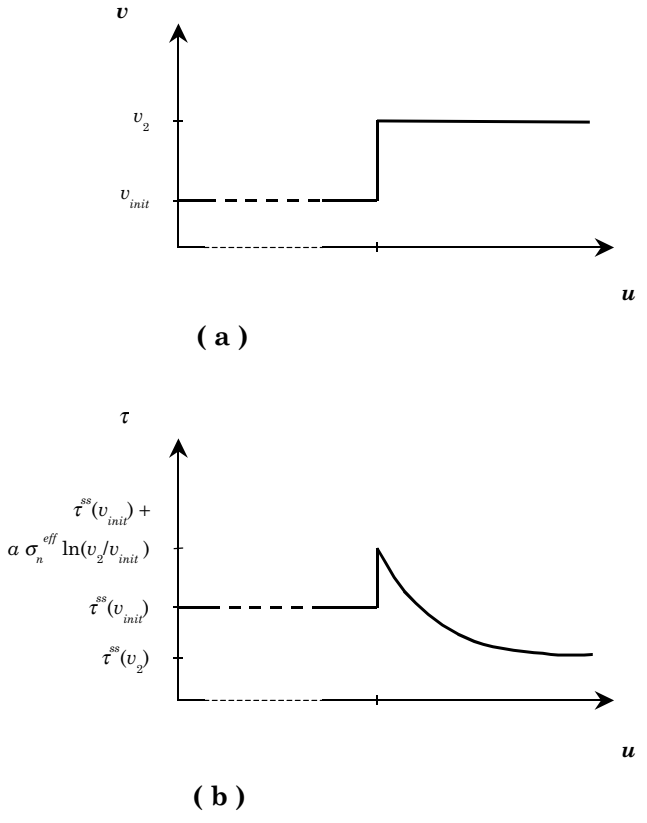

Figure 8. Effect of an abrupt change of the slip velocity (a) on the friction (shown in b, redrawn after Gu *et al.* 1984). When the load velocity suddenly jumps from an initial value to the level v_2, the friction τ reaches a peak value and then exponentially decreases for large values of the slip.

friction is at steady state. We have verified that in the final configuration the state variable Φ does not change with time; to show this we have plotted in Fig. 11 the phase diagram (i.e. shear traction versus slip velocity) for the DR law at the fault position $x_1 = 11.8$. The intersections with the steady-state line $\tau^{ss}(v)$ show that at the end of the stress release, τ is in the steady state.

The temporal evolution of total traction and its behaviour as a function of slip and slip velocity resulting from the two constitutive formulations are shown in Fig. 12 for the same gridpoint as the one used for Fig. 11. The time evolution of total traction (Fig. 12a) indicates that the two constitutive laws provide similar trends. It is important to consider that, in the selected position along the fracture line ($x_1 = 11.8$), the crack tip is split only for the SW solution. This explains the higher peak of the total traction resulting from the SW law and its earlier drop to the kinetic level τ_f. The solution resulting from the DR law shows some oscillations before and after the traction drop. This behaviour is also evident in the phase diagram shown in Fig. 12(d). We emphasize that the two solutions yield the same stress drop ($\tau_0 - \tau_f$), confirming that the association between constitutive parameters is correct.

Figs 12(b) and (c) show the total traction as a function of slip: worthy of note is that the SW behaviour is common to both solutions. However, while (as expected) the SW solution shows only a weakening phase, that is, traction always decreases for increasing slip, the DR solution has a slip-hardening phase preceding the weakening stage. We remark that this behaviour is much more general than that resulting from the SW solution. According to Ionescu & Campillo (1999) the initial value of friction is a key parameter in controlling the nucleation process. We emphasize that the solution resulting from the rate- and state-dependent law may contain this initial increase of traction for increasing slip (direct effect); this implies more general behaviour during the nucleation stage.

In conclusion, we believe that the rate- and state-dependent friction laws reproduce the results obtained with an SW constitutive relation and that they allow one to model an extensive class of phenomena concerning the frictional behaviour of faults that includes aseismic slip and creep as well as coupling and interactions between different frictional regimes (Rice 1993; Boatwright & Cocco 1996; Gomberg *et al.* 1998).

6 HETEROGENEOUS DISTRIBUTION OF FRICTIONAL PARAMETERS IN RATE- AND STATE-DEPENDENT LAWS

In Section 4.2 we discussed several simulations in order to compare the behaviour obtained with the BIE and the FD numerical methods by applying the SW governing equation with a heterogeneous distribution of constitutive parameters. In particular, we have examined a model where the rupture is arrested by a barrier and a healing phase back-propagates along the fractured zone (Fig. 6). This behaviour has been defined as barrier-healing.

In this section we aim to present some simulations calculated by using the FD method and heterogeneous spatial distributions of constitutive parameters for the DR law. In particular, we discuss the inference on the rupture arrest of using rate- and state-dependent constitutive laws, emphasizing the effects of fault heterogeneities.

6.1 Inference on the rupture arrest

One of the most important implications of barrier-healing models is that the slip duration is variable along the fault: this duration depends of the distance of the gridpoint from the barrier or the crack edge. The further the point is from the barrier, the larger the slip durations are expected to be (with a null duration at the crack edge). More recently, an alternative model has been proposed, which consists of short and possibly constant slip durations during the rupture growth (e.g. Heaton 1990; Olsen *et al.* 1997); it is usually called self-healing. While barrier-healing is simulated by classical crack models (see Day 1982; Das & Kostrov 1983), the theoretical modelling of the self-healing process requires the use of more complex constitutive formulations. Several recent studies have modelled the self-healing process (e.g. Perrin *et al.* 1995; Cochard & Madariaga 1994; Zheng & Rice 1998) by using different constitutive laws that involve fault re-strengthening at very small velocities also. Many other authors have proposed different regularizations of the rate- and state-dependent constitutive laws in order to eliminate the singularity in the governing equation at the stationary contact (the slip velocity is zero; see Perrin *et al.* 1995; Roy & Marone 1996; Zheng & Rice 1998). In fact, the propagation of a true pulse of slip velocity implies a zero velocity behind the rupture front, and it is therefore possible only with regularized laws. In this study we aim to focus on the role played by heterogeneous distributions of constitutive

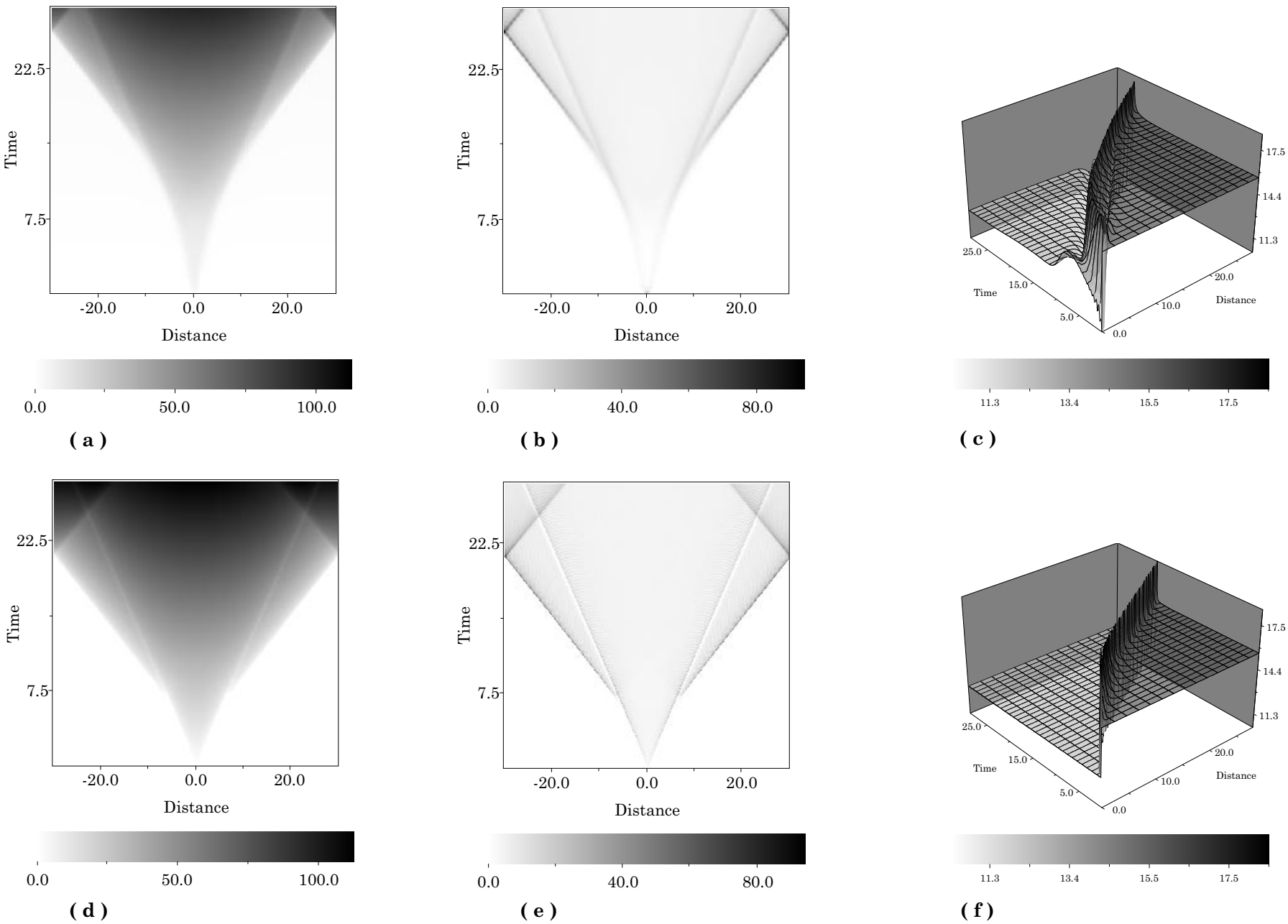

Figure 9. (a) Slip, (b) slip velocity and (c) a 3-D view of traction obtained by an FD approach and using the DR constitutive equation. The frictional behaviour is characterized by $B-A \gg 0$ and it is very velocity-weakening or strong seismic. (d), (e) and (f) show the same solutions obtained by using the FD approach using an SW law with $S<1.77$ (see Table 1 for details of the constitutive parameters).

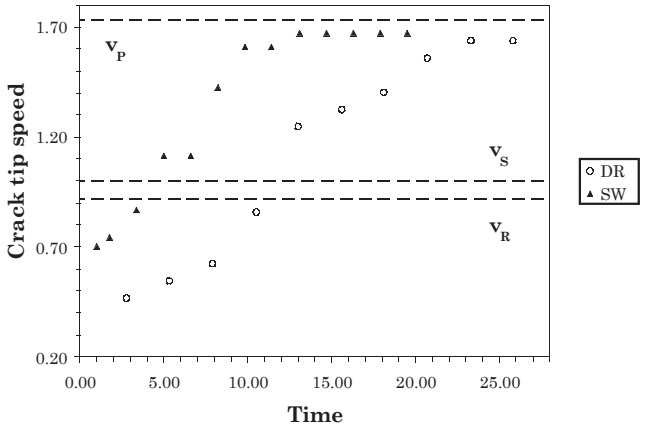

Figure 10. Behaviour of the crack speed (velocity of the tip) versus time obtained with the DR (open circles) and SW friction laws (solid triangles). After an initial increase over v_S the crack speed asymptotically reaches v_P.

parameters and we propose also that in this configuration different healing mechanisms can be simulated, even using the DR law without any regularization.

We present the modelling results of three different configurations. The first is a homogeneous distribution of constitutive parameters, in the second one we assume that only the parameter L of the DR law is heterogeneous along the fault, while in the third configuration both parameters a and b change along the fault line while L remains constant. We show the results of these simulations in Fig. 13 by plotting the slip as a function of crack position as a superposition of snapshots at different time steps and in Fig. 14 by 3-D plots of the spatio–temporal evolution of slip velocity.

The first configuration allows us to simulate a classical enlarging crack where the rupture arrest in not modelled (Fig. 13a) and slip grows continuously as the crack advances along the line. We use this only as a reference model, since it is not of interest in this study. Fig. 14(a) clearly shows the

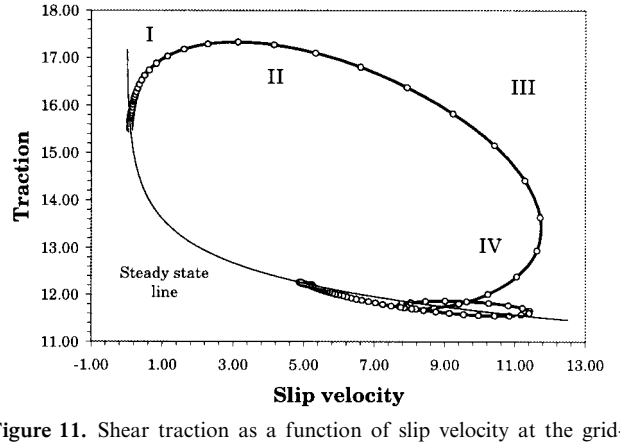

Figure 11. Shear traction as a function of slip velocity at the gridpoint $x_1 = 11.8$ for the DR law. The steady-state curve is plotted. This indicates that the traction is, at the end of the process, in the steady state. The numbers identify the different stages of the dynamic rupture. I: velocity-hardening; II: dynamic acceleration; III: stress release; IV: crack deceleration. The secondary loop after stage IV is due to the second rupture front propagating at v_R since at this gridpoint the rupture bifurcation has already occurred.

evolution of slip velocity for a barrier-healing model: slip at each gridpoint grows until the arrival of the back-propagating healing front. This behaviour is also clear in Fig. 13(b), which shows the snapshots of slip as a function of crack position. The barrier has been simulated using a greater value of the L parameter outside the rupturing region. The simulation shown in Figs 13(c) and 14(b) has been computed by assuming a heterogeneous distribution of the a and b parameters: the area where the rupture is propagating is velocity-weakening and it is surrounded by a velocity-strengthening area.

The resulting slip duration is much shorter than that obtained for barrier-healing, although it is not constant, as evidenced by the shape of the healing front in Fig. 14(b). This rupture behaviour is due to a self-healing mechanism that occurs during crack propagation. These figures clearly indicate the differences between barrier-healing and self-healing models: the latter implies a shorter slip duration. To emphasize this behaviour, we plot in Fig. 15 the slip velocity time histories at four different gridpoints where the slip duration is nearly constant.

In the latter model it is quite evident that the rupture, at a specific gridpoint, heals before the arrival of the rupture front back-propagating from the velocity-strengthening region. We emphasize that in this study we have modelled both a barrier-healing and a self-healing mechanism simply by assuming heterogeneous distributions of constitutive parameters.

7 THE NUCLEATION PHASE

In this section we discuss the effects of using different sets of constitutive parameters on the nucleation process. The duration of the nucleation phase has been experimentally defined by using ground-motion recordings (Ellsworth & Beroza 1995; Beroza & Ellsworth 1996) and laboratory experiments on fault friction (Dieterich 1992; Dieterich & Kilgore 1996; Ohnaka 1993 and references therein), and has been theoretically explained by using both SW behaviour (Ohnaka & Yamashita 1989; Ionescu & Campillo 1999) and rate- and state-dependent friction laws (Okubo & Dieterich 1986; Dieterich 1994). Shibazaki & Matsu'ura (1998) and Ohnaka (1993) described the phase preceding the dynamic propagation at very high speeds ($v_{\rm crack} \geq 2$ km s^{-1}) as a very slow quasi-static process ($v_{\rm crack} \cong 1$ cm s^{-1}) followed by a quasi-dynamic but still slow ($v_{\rm crack} \cong 10$ m s^{-1}) enlargement that does not radiate seismic waves (see Fig. 11 in Shibazaki & Matsu'ura 1998). This implies that the quasi-dynamic phase proposed by these authors is distinct from that identified by Beroza & Ellsworth (1996) on recorded seismograms. The beginning of the first slow quasi-static phase is unknown, therefore the definition of nucleation duration accounts only for the two latter phases of quasi-dynamic and fully dynamic rupture growth.

Umeda (1992), Ellsworth & Beroza (1995) and Shibazaki & Matsu'ura (1998) proposed a relation between the duration of the nucleation phase and the total seismic moment of the final event. Roy & Marone (1996) used a spring-slider model and defined the duration as the time during which the system evolution is quasi-static and is not yet inertia dominated. This definition is in quite good agreement with the previous ones. Dieterich (1986) identified the duration of the nucleation process as a first phase in which the crack half-length l is less than the critical half-length l_c (see the definition in Appendix D) and the slip is intrinsically stable, and a second phase, in which $l > l_c$, characterized by a progressive acceleration up to dynamic

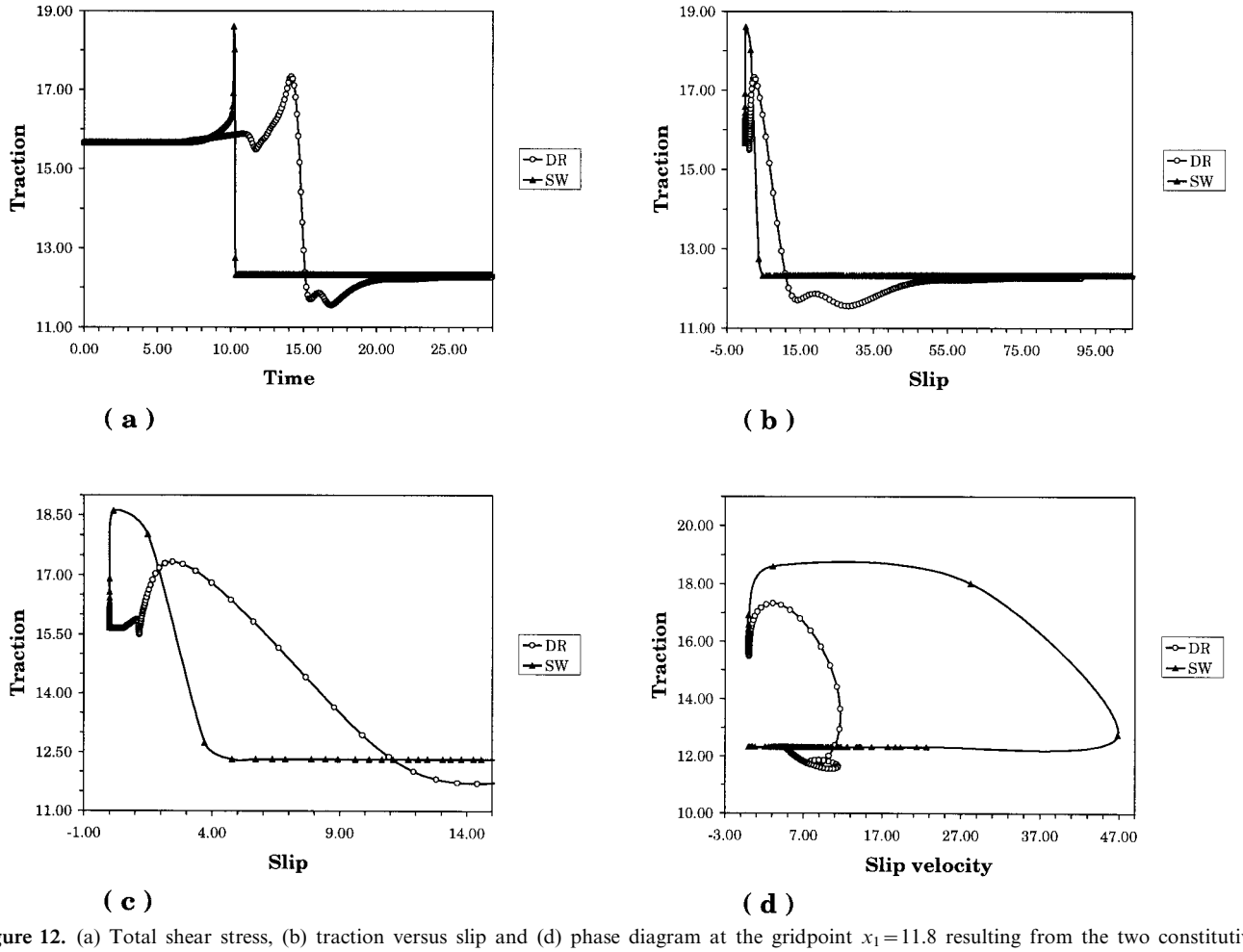

Figure 12. (a) Total shear stress, (b) traction versus slip and (d) phase diagram at the gridpoint $x_1 = 11.8$ resulting from the two constitutive equations. The constitutive parameters are those used in Fig. 9. (c) displays an enlargement of the traction behaviour as a function of slip during the breakdown process.

instability. This definition was also used by Ionescu & Campillo (1999). Ohnaka & Shen (1999) pointed out the correlation existing between the propagation velocity fields and the rate l/l_c.

According to Dieterich (1986), we define in this paper the duration T_n of the nucleation phase as the time necessary for the crack half-length to reach l_c. The analytical expression for the critical length l_c is given in Appendix D both for the SW model and for the DR formulation. Therefore, because l_c depends on the constitutive parameters, T_n also depends on the frictional properties of the fault.

In this study we aim to understand how such different constitutive laws and the variability of their parameters influence the nucleation phase. By using the FD approach, we have performed a large number of numerical tests that satisfy all the stability conditions (Appendix C). In particular, we have studied some relations between the duration T_n and the nucleation seismic moment M_{0n}, the critical half-length l_c and the constitutive distance L or d_0 (Fig. 16). The nucleation seismic moment M_{0n} is defined by accounting for the amount of slip in the nucleation region. We have performed several simulations using the DR law and choosing different values of the constitutive parameters: a and b range between 0.75 and 1.12 and between 1.41 and 1.625, respectively, and L between 1. and 1.6. In this way we obtain different values of l_c and therefore different T_n. In the simulations performed using SW we have varied the constitutive parameters τ_u (between 1.05 and 1.8) and d_0 (between 0.6 and 2.8). The initial shear stress τ_0 and the kinetic friction τ_f are constant for all simulations; they are 1 and 0, respectively. In this way we change the strength parameter S and/or the characteristic length. We first investigate the dependence of M_{0n} on T_n (Fig. 16a). Both methods exhibit a nearly linear scaling of these parameters. However, the DR law predicts larger values of M_{0n} than the SW law, and, more interestingly, the DR simulations show a variability and dependence on the constitutive parameters. In Fig. 16(a) we have indicated with solid circles the values corresponding to those simulations where a and b are constants and only L is changed; this yields a linear scaling between nucleation time and seismic moment. The open circles in Fig. 16(a) show the values resulting from those simulations in which L is constant while a and b vary. The upper values correspond to those cases where the difference $b-a$ is large ($b=1.6$ and a in the range [0.75, 0.9]—very strong unstable behaviour), while the lower values correspond to those where $b-a$ is smaller (weak seismic behaviour). This figure shows that the nucleation seismic moment depends on the difference $b-a$. A linear relation between M_{0n} and T_n as a function of the critical distance has been found using both the SW (solid triangles) and the DR (solid circles) laws. The latter yields larger values of the nucleation seismic moment. The variations of b and a in the DR law yield

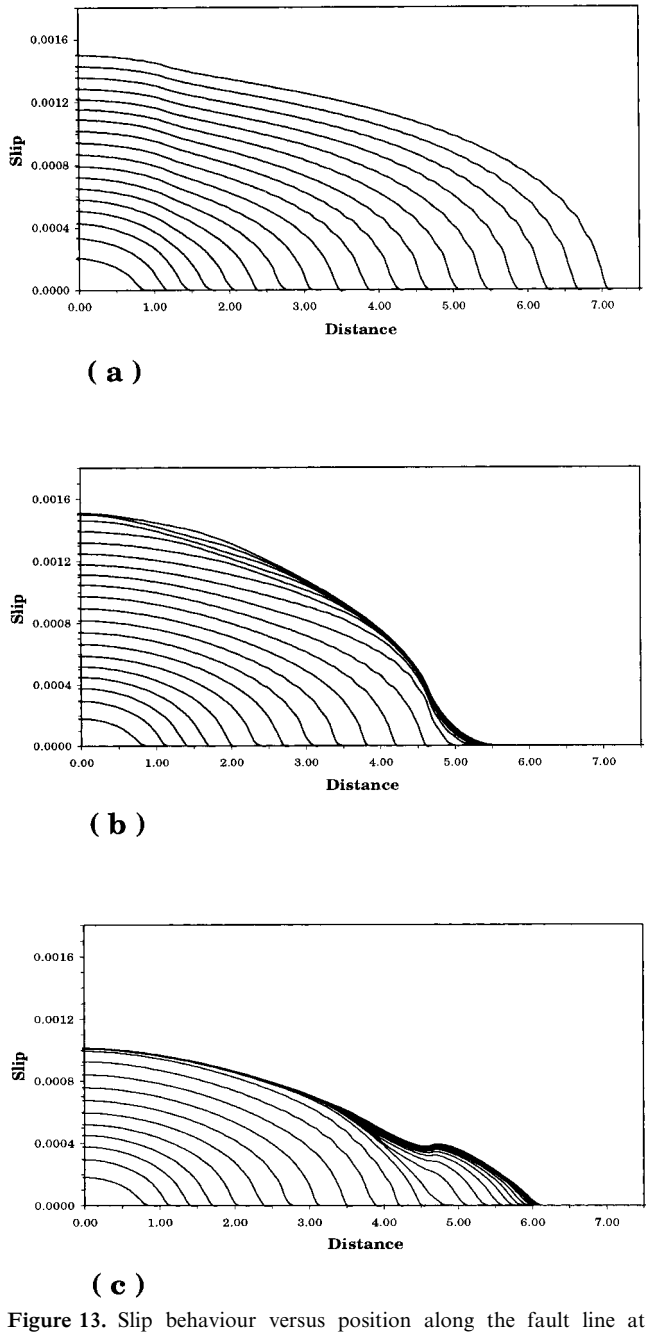

Figure 13. Slip behaviour versus position along the fault line at different time steps (each line is a slip snapshot). (a) Reference homogeneous case, representing a classical velocity-weakening model ($a=0.012$, $b=0.016$, $L=1\times10^{-5}$ m). (b) Heterogeneous model where only the parameter L is variable, a and b being the same as in (a) and $L=1\times10^{-2}$ m for $x_1\geq5$ m. We refer to this as a barrier-healing model. (c) Heterogeneous model where L is uniform along the fault, but not a and b: after $x_1=5$ m they become $a=0.015$, $b=0.012$. This corresponds to a velocity-strengthening region. We refer to this as a self-healing model. The scale of the abscissa is the same in the three cases and values are expressed in metres.

a different slope in the scaling law from that obtained by changing L. These results can be explained by considering that the different frictional parameters (a, b and L) have different effects on the frictional behaviour of faulting.

A linear correlation is also found between T_n and l_c (Fig. 16b). In the SW case the result is $T_n\cong3l_c/2v_S$, consistent with the relation derived by Shibazaki & Matsu'ura (1998), while in the DR case we obtain $T_n\cong3.3l_c/v_S$. In the latter case we found a greater dispersion. The difference between the slopes in the two trends shown in Fig. 16(b) shows that the SW law predicts a propagation velocity in the quasi-static nucleation phase (roughly expressed by $v_{crack}\cong l_c/T_n$) greater than that resulting from a DR law. By maintaining constant a and b in the DR law as well as S in the SW relation, we have shown in Fig. 16(c) the link existing between T_n and L or d_0. The correlation is still linear in both constitutive models, although with different slopes.

These modelling results clearly show that SW and rate- and state-dependent constitutive laws yield different behaviours during the nucleation phase. Nevertheless, it is important to remember that the SW law used in this study has a constant weakening rate depending on the constitutive initial parameters assumed. According to Ionescu & Campillo (1999), if variable weakening rates and/or different values for the initial slope of the SW curve are used, more complex behaviour for the nucleation phase is expected. However, we emphasize that such more complex trends of the SW curves are well predicted by the rate- and state-dependent friction laws. Therefore, the variability of the nucleation parameters resulting from this constitutive formalism should include and agree with the results of Ionescu & Campillo (1999).

8 DISCUSSION AND CONCLUSIONS

In this paper we have shown comparisons between the solutions of the dynamic problem for a planar 2-D shear crack using two different numerical methods: a boundary integral equation method (BIE), originally proposed by Andrews (1985), and a finite different approach (FD), first proposed by Andrews (1973). We have also used different constitutive equations, which include the classical SW model and rate- and state-dependent friction laws (DR).

The comparison between the two numerical procedures indicates that the two methods yield similar solutions when the stability conditions are satisfied. Both BIE and FD methods provide similar time histories for the slip, slip velocity and shear traction. In particular, we emphasize the necessity of verifying the stability conditions and the resolution of the cohesive zone by also looking at the behaviour of total traction versus slip and slip velocity (we refer to this latter as the phase diagram). Under these conditions the peak slip velocities predicted by the two approaches are in good agreement. Both solutions resulting from the BIE and the FD methods show crack bifurcation and the expected behaviour for the rupture propagation of a 2-D in-plane crack. The main differences are found inside the nucleation zone and at the rupture bifurcation, when the rupture velocity tends to the P-wave velocity. The BIE algorithm we used for our simulations is faster that our FD code.

We have also compared numerical solutions resulting from both an SW and a DR constitutive formulation. This comparison requires that the initial values of the constitutive parameters are properly chosen. We have suggested a physically reliable association between initial parameters for the two governing equations. The comparison between the two constitutive formulations has shown that rate- and state-dependent friction laws also yield an SW behaviour, although much more general than that used in our formulation of the SW law.

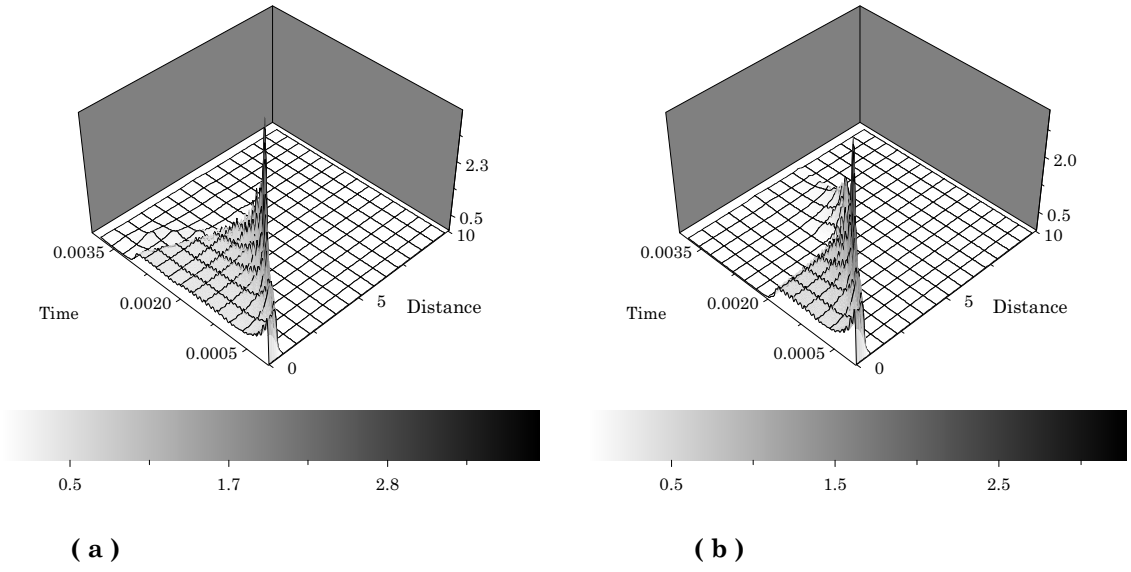

Figure 14. (a), (b) 3-D views of slip velocity for the heterogeneous models described in Figs 13(b), (c), respectively. Time is expressed in seconds, distance in metres and slip velocity in metres per second.

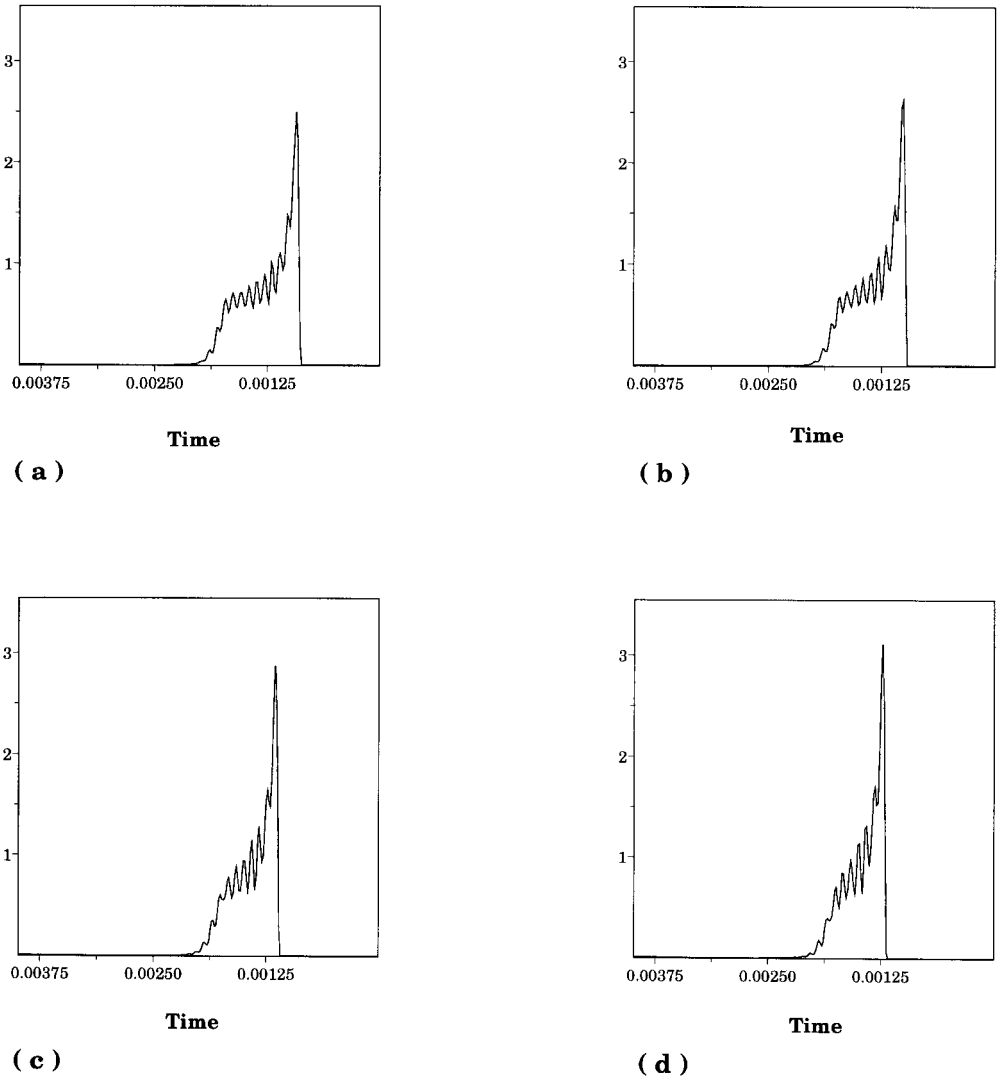

Figure 15. Slip velocity versus time at different fault points: (a) $x_1 = 2.2$, (b) $x_1 = 2.4$, (c) $x_1 = 2.7$, (d) $x_1 = 2.9$ for the heterogeneous configuration of Figs 13(c) and 14(b). The slip duration shows a self-healing behaviour. Time is expressed in seconds and slip velocity in metres per second.

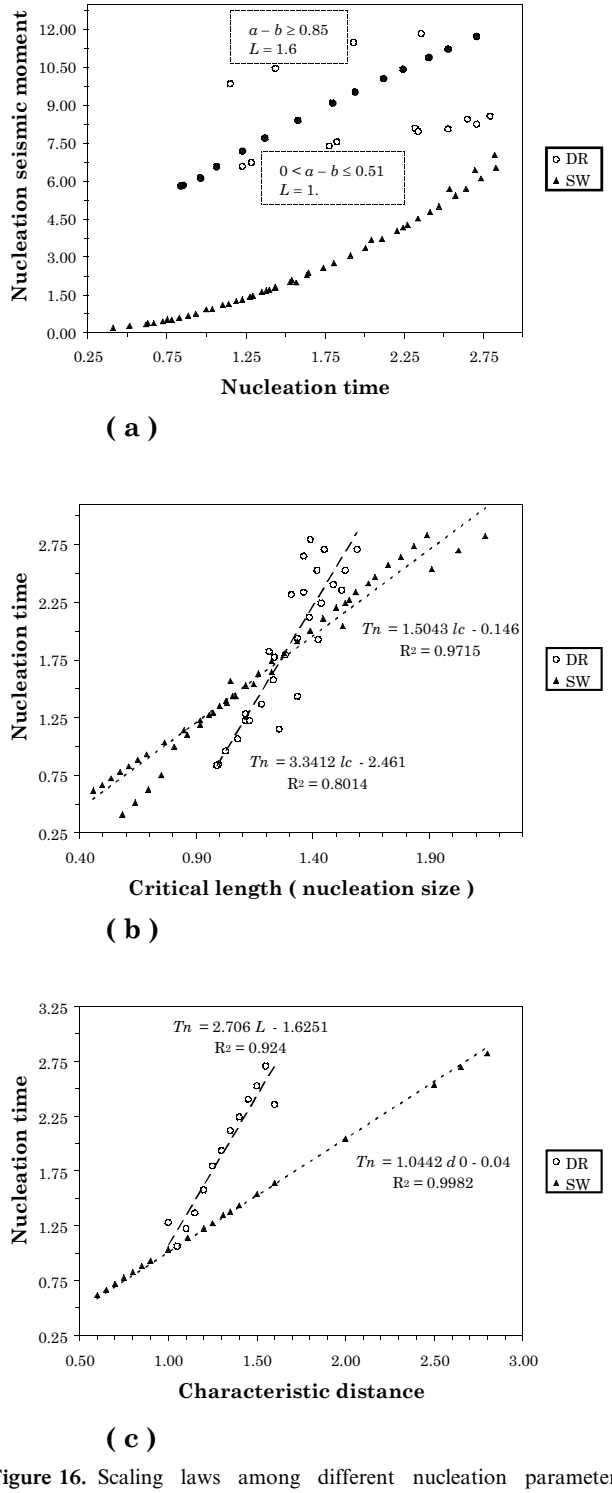

Figure 16. Scaling laws among different nucleation parameters inferred by using the SW and DR constitutive equations derived for homogeneous configurations. For all simulations, which are performed by the FD method, the convergence–stability conditions (Appendix C) are satisfied. (a) Nucleation seismic moment versus nucleation time; for the DR case, we represent with solid circles the configurations in which a and b are constant (varying only L), while open circles show the values resulting from constant L and variable a and b. These values depict two trends associated with large and small $b-a$, respectively. Nucleation time versus (b) critical length and (c) characteristic distance. For the evaluation of the critical half-length l_c we have chosen the parameter η of eq. (D7) to be 2/3, in agreement with Dieterich (1992). R^2 is the square of Pearson's correlation coefficient.

In fact, the SW behaviour resulting from a rate- and state-dependent friction law can include an initial slip-hardening phase that is due to the direct effect of friction and not to the evolution of the state variable. This avoids the subjective choice of the initial value of the weakening rate, which according to Ionescu & Campillo (1999) controls the duration of the nucleation phase.

The comparison between numerical simulations resulting from the SW and DR laws shows a similar behaviour for the rupture propagation but a very different behaviour for the initial quasi-static rupture growth during the nucleation stage. We also observe a crack bifurcation and a jump in rupture velocity towards the *P*-wave speed by using the DR constitutive law. However, while the SW law yields a sudden rupture acceleration, corresponding to dynamic propagation immediately after the imposed nucleation, the DR law (and in general the rate- and state-dependent laws) produces an initial quasi-dynamic phase where the rupture accelerates but at a slow velocity. This is evident from a comparison of the rupture velocities during the crack growth resulting from the two constitutive formulations. This different nucleation behaviour implies that the crack bifurcation for the simulations with the DR law occurs later than that resulting from the SW law. We have also verified that the initial and final values of the total traction for the DR law correspond to steady-state values.

We point out that the DR law allows us to describe and model a wide class of frictional behaviours. This emphasizes the importance of studying the mutual interaction between fault patches characterized by different frictional properties, as already pointed out by Boatwright & Cocco (1996) by using a simple spring-slider dynamic system. These investigations in two or three dimensions will be the subject of a future work.

In this study we have implemented the numerical codes to allow heterogeneous distributions of the constitutive parameters. We have performed several simulations using an SW law and heterogeneous distributions of the stress parameters as well as of the critical slip distance d_0. The spatial variation of fault strength or stress drop yields the expected variability of the rupture velocity during crack growth, already modelled by previous studies (Day 1982; Das & Kostrov 1983) and in three dimensions by Fukuyama & Madariaga (1998) and Madariaga *et al.* (1998). We have reproduced the rupture arrest caused by a barrier, which is a typical solution in fracture mechanics. We refer to this behaviour as barrier-healing in order to emphasize that the arrest mechanism caused by the back-propagating healing front yields variable rise times (Madariaga *et al.* 1998). The slip duration is therefore greatest in the centre of the crack and smallest near the crack edge or at the barrier.

We have also performed several simulations using spatially heterogeneous distributions of the constitutive parameters for the DR law. By using a heterogeneous distribution of the characteristic distance L in the DR law, we have also reproduced the barrier-healing with the rate- and state-dependent law. However, this constitutive formulation allows for a more general behaviour. We have simulated a self-healing mechanism, which implies a short slip duration (e.g. Heaton 1990; Madariaga & Cochard 1994; Perrin *et al.* 1995; Zheng & Rice 1998) by allowing the heterogeneity of the constitutive parameters a and b.

This conclusion is particularly important because it indicates that if we consider the spatial variability of constitutive parameters (Rice 1993; Boatwright & Cocco 1996) and we model

short but not constant slip durations, we do not need the numerous regularizations of the governing equations that have been proposed in literature to simulate the self-healing process. It also emphasizes the importance of the parameter L, which provides the scaling law from experimental to actual faults. Dieterich & Kilgore (1996) noticed, in fact, that in the laboratory, L increases with the gauge particle size and the surface roughness. Because in nature faults are much less smooth, it appears plausible that real faults may have much greater values of L (Ide & Takeo 1997; Olsen *et al*. 1997). We conclude that the heterogeneity of the constitutive parameters can explain many of the dynamic features of seismic faults (such as the rupture nucleation and arrest) by using the same theoretical formulation.

Finally, by using different sets of constitutive parameters we have investigated how the nucleation duration scales with the characteristic distance, the critical length (that is, the nucleation dimension) and the seismic moment of the nucleation patch. We reproduced the scaling law proposed by Shibazaki & Matsu'ura (1998) by using the SW law and we obtained a similar scaling law for the DR constitutive relations. We found characteristic differences between the SW and DR laws. The latter provides more complex behaviour.

REFERENCES

Aki, K., 1979. Characterization of barriers on an earthquake fault, *J. geophys. Res.,* **84,** 6140–6148.

Andrews, D.J., 1973. A numerical study of tectonic stress release by underground explosions, *Bull. seism. Soc. Am.,* **63,** 1375–1391.

Andrews, D.J., 1976a. Rupture propagation with finite stress in antiplane strain, *J. geophys. Res.,* **81,** 3575–3582.

Andrews, D.J., 1976b. Rupture velocity of plane strain shear cracks, *J. geophys. Res.,* **81,** 5679–5687.

Andrews, D.J., 1985. Dynamic plane-strain shear rupture with a slip-weakening friction law calculated by a boundary integral method, *Bull. seism. Soc. Am.,* **75,** 1–21.

Andrews, D.J., 1994. Dynamic growth of mixed-mode shear cracks, *Bull. seism. Soc. Am.,* **84,** 1184–1198.

Andrews, D.J. & Ben-Zion, Y., 1997. Wrinkle-like slip pulse on a fault between different materials, *J. geophys. Res.,* **102,** 553–571.

Barenblatt, G.I., 1959a. The formation of equilibrium cracks during brittle fracture. General ideas and hypothesis. Axially symmetric cracks, *Appl. Math. Mech.,* **23,** 662–636.

Barenblatt, G.I., 1959b. Concerning equilibrium crack forming during brittle fracture. The stability of isolated cracks. Relationship with energetic theories, *Appl. Math. Mech.,* **23,** 1273–1282.

Beeler, N.M., Tullis, T.E. & Weeks, J.D., 1994. The roles of time and displacement in the evolution effect in rock friction, *Geophys. Res. Lett.,* **21,** 1987–1990.

Ben-Zion, Y. & Andrews, D.J., 1998. Properties and implications of dynamic rupture along a material interface, *Bull. seism. Soc. Am.,* **88,** 1085–1094.

Beroza, G.C. & Ellsworth, W.L., 1996. Properties of the seismic nucleation phase, *Tectonophysics,* **261,** 209–227.

Boatwright, J. & Cocco, M., 1996. Frictional constraints on crustal faulting, *J. geophys. Res.,* **101,** 13 895–13 909.

Bouchon, M., Sekiguchi, H., Irikura, K. & Iwata, T., 1998. Some characteristics of the stress field of the 1995 Hyogo-ken Nanbu (Kobe) earthquake, *J. geophys. Res.,* **103,** 24 271–24 282.

Campillo, M. & Ionescu, I.R., 1997. Initiation of antiplane shear instability under slip dependent friction, *J. geophys. Res.,* **102,** 20 363–20 371.

Carlson, J.M. & Langer, J.S., 1989. Mechanical model of an earthquake fault, *Phys. Rev. A Gen. Phys.,* **40,** 6470–6484.

Cochard, A. & Madariaga, R., 1994. Dynamic faulting under rate-dependent friction, *Pure appl. Geophys.,* **142,** 419–445.

Das, S. & Aki, K., 1977a. A numerical study of two-dimensional spontaneous rupture propagation, *Geophys. J. R. astr. Soc.,* **50,** 643–668.

Das, S. & Aki, K., 1977b. Fault plane with barriers: a versatile earthquake model, *J. geophys. Res.,* **82,** 5658–5670.

Das, S. & Kostrov, B.V., 1983. Breaking of a single asperity: rupture process and seismic radiation, *J. geophys. Res.,* **88,** 4277–4288.

Day, S.M., 1982. Three-dimensional finite difference simulation of fault dynamics: rectangular faults with fixed rupture velocity, *Bull. seism. Soc. Am.,* **72,** 705–727.

Dieterich, J.H., 1986. A model for the nucleation of earthquake slip, in *Earthquake Source Mechanics, Geophysical Monograph,* Vol. 37, Maurice Ewing Ser. 6, pp. 37–47, eds Das, S., Boatwright, J. & Scholz, C.H., AGU, Washington, DC.

Dieterich, J.H., 1992. Earthquake nucleation on faults with rate- and state-dependent strength, *Tectonophysics,* **211,** 115–134.

Dieterich, J.H., 1994. A constitutive law for rate of earthquake production and its application to earthquake clustering, *J. geophys. Res.,* **99,** 2601–2618.

Dieterich, J.H. & Kilgore, B., 1996. Implications of fault constitutive properties for earthquake prediction, *Proc. Nat. Acad. Sci. USA,* **93,** 3787–3794.

Ellsworth, W.L. & Beroza, G.C., 1995. Seismic evidence for an earthquake nucleation phase, *Science,* **268,** 851–855.

Fukuyama, E. & Madariaga, R., 1998. Rupture dynamics of a planar fault in a 3D elastic medium: rate- and slip-weakening friction, *Bull. seism. Soc. Am.,* **88,** 1–17.

Gomberg, J., Beeler, N., Blanpied, M. & Bodin, P., 1998. Earthquake triggering by transient and static deformations, *J. geophys. Res.,* **103,** 24 411–24 426.

Gu, J.C., Rice, J.R., Ruina, A.L. & Tse, S.T., 1984. Slip motion and stability of a single degree of freedom elastic system with rate and state dependent friction, *J. Mech. Phys. Sol.,* **32,** 167–196.

Guatteri, M. & Spudich, P., 2000. What can strong-motion data tell us about slip-weakening fault-friction?, *Bull. seism. Soc. Am.,* **90,** 98–116.

Harris, R.A. & Day, S.M., 1997. Effects of a low-velocity zone on a dynamic rupture, *Bull. seism. Soc. Am.,* **87,** 1267–1280.

Heaton, T.H., 1990. Evidence for and implications of self-healing pulses of slip in earthquake rupture, *Phys. Earth planet. Inter.,* **64,** 1–20.

Ida, Y., 1972. Cohesive force across the tip of a longitudinal-shear crack and Griffith's specific surface energy, *J. geophys. Res.,* **77,** 3796–3805.

Ide, S. & Takeo, M., 1997. Determination of constitutive relations of fault slip based on seismic wave analysis, *J. geophys. Res.,* **102,** 27 379–27 391.

Iio, Y., 1995. Observations of slow initial phase generated by micro-earthquakes: implications for earthquake nucleation and propagation, *J. geophys. Res.,* **100,** 15 333–15 349.

Ionescu, I.R. & Campillo, M., 1999. Influence of the shape of the friction law and fault finiteness on the duration of initiation, *J. geophys. Res.,* **104,** 3013–3024.

Kostrov, B.V. & Das, S., 1988. Principles of earthquake source mechanics, *Cambridge Monogr. Mech. appl. Math.,* Cambridge University Press, Cambridge.

Linker, M.F. & Dieterich, J.H., 1992. Effects of variable normal stress on rock friction: observations and constitutive equations, *J. geophys. Res.,* **97,** 4923–4940.

Madariaga, R. & Cochard, A., 1994. Seismic source dynamics, heterogeneity and friction, *Ann. Geof.,* **37,** 1349–1375.

Madariaga, R., Olsen, K. & Archuleta, R., 1998. Modeling dynamic rupture in a 3D earthquake fault model, *Bull. seism. Soc. Am.,* **88,** 1182–1197.

Marone, C., 1998. Laboratory-derived friction laws and their application to seismic faulting, *Ann. Rev. Earth planet. Sci.,* **26,** 643–696.

Marone, C. & Scholz, C.H., 1988. The depth of seismic faulting and the upper transition from stable to unstable slip regimes, *Geophys. Res. Lett.,* **15,** 621–624.
Matsu'ura, M., Kataoka, H. & Shibazaki, B., 1992. Slip-dependent friction law and nucleation processes in earthquake rupture, *Tectonophysics,* **211,** 135–148.
Mikumo, T., 1992. Dynamic fault rupture and stress recovery processes in continental crust under depth-dependent shear strength and frictional parameters, *Tectonophysics,* **211,** 201–222.
Nielsen, S.B., Carlson, J.M. & Olsen, K.B., 2000. Influence of friction and fault geometry on earthquake rupture, *J. geophys. Res.,* **105,** 6069–6088.
Nostro, C., Piersanti, A., Antonioli, A. & Spada, G., 1999. Spherical versus flat models of coseismic and postseismic deformations, *J. geophys. Res.,* **104,** 13 115–13 134.
Ohnaka, M., 1993. Critical size of the nucleation zone of earthquake rupture inferred from immediate foreshock activity, *J. Phys. Earth,* **41,** 45–56.
Ohnaka, M., 1996. Nonuniformity of the constitutive law parameters for shear rupture and quasistatic nucleation to dynamic rupture: a physical model of earthquake generation processes, *Proc. Nat. Acad. Sci. USA,* **93,** 3795–3802.
Ohnaka, M. & Shen, L., 1999. Scaling of the shear rupture process from nucleation to dynamic propagation: implications of geometric irregularity of the rupturing surfaces, *J. geophys. Res.,* **104,** 817–844.
Ohnaka, M. & Yamashita, T., 1989. A cohesive zone model for dynamic shear faulting based on experimentally inferred constitutive relation and strong motion source parameters, *J. geophys. Res.,* **94,** 4089–4104.
Okubo, P.G., 1989. Dynamic rupture modeling with laboratory-derived constitutive relations, *J. geophys. Res.,* **94,** 12 321–12 335.
Okubo, P.G. & Dieterich, J.H., 1986. State variable fault constitutive relations for dynamic slip, *Earthquake Source Mechanics, Geophysical Monograph*, Vol. 37, Maurice Ewing Ser. 6, pp. 25–35, eds Das, S., Boatwright, J. & Scholz, C., AGU, Washington, DC.
Olsen, K.B., Madariaga, R. & Archuleta, R.J., 1997. Three-dimensional dynamic simulation of the 1992 Landers earthquake, *Science,* **278,** 834–838.
Papageorgiou, A.S. & Aki, K., 1983. A specific barrier model for the quantitative description of inhomogeneous faulting and the prediction of strong ground motion, Part II, Application of the model, *Bull. seism. Soc. Am.,* **73,** 953–978.
Perfettini, H., Stein, R.S., Simpson, R. & Cocco, M., 1999. Stress transfer by the 1988–89 $M=5.3$ and 5.4 Lake Elsman foreshocks to the Loma Prieta fault: unclamping at the site of peak mainshock slip, *J. geophys. Res.,* **104,** 20 169–20 182.
Perrin, G., Rice, J.R. & Zheng, G., 1995. Self-healing slip pulse on a frictional surface, *J. Mech. Phys. Sol.,* **43,** 1461–1495.
Petschek, A.G. & Hanson, M.E., 1968. Difference equation for two-dimensional elastic flow, *J. Comp. Phys.,* **3,** 307.
Press, W.H., Teukolsky, S.A., Vetterling, W.T. & Flannery, B.P., 1992. *Numerical Recipes in FORTRAN. The Art of Scientific Computing,* 2nd edn, Cambridge University Press, Cambridge.
Ranjith, K. & Rice, J.R., 1999. Stability of quasi-static slip in a single degree of freedom elastic system with rate and state dependent friction, *J. Mech. Phys. Sol.,* **47,** 1207–1218.
Rice, J.R., 1993. Spatio-temporal complexity of slip on a fault, *J. geophys. Res.,* **98,** 9885–9907.
Rice, J.R. & Ben-Zion, Y., 1996. Slip complexity in earthquake fault models, *Proc. Nat. Acad. Sci. USA,* **93,** 3811–3818.
Rice, J.R. & Ruina, A.L., 1983. Stability of steady frictional slipping, *J. appl. Mech.,* **50,** 343–349.
Rice, J.R. & Tse, S.T., 1986. Dynamic motion of a single degree of freedom system following a rate and state dependent friction law, *J. geophys. Res.,* **91,** 521–530.
Roy, M. & Marone, C., 1996. Earthquake nucleation on model faults with rate- and state-dependent friction: effects of inertia, *J. geophys. Res.,* **101,** 13 919–13 932.
Ruina, A.L., 1980. Friction laws and instabilities: a quasistatic analysis of some dry frictional behavior, *PhD thesis,* Brown University, Providence, RI.
Ruina, A.L., 1983. Slip instability and state variable friction laws, *J. geophys. Res.,* **88,** 10 359–10 370.
Shibazaki, B. & Matsu'ura, M., 1998. Transition process from nucleation to high-speed rupture propagation: scaling from stick-slip experiments to natural earthquakes, *Geophys. J. Int.,* **132,** 14–30.
Trulio, J.G., 1964. Studies of finite difference techniques for continuum mechanics, *Technical Documentary,* Rept WLTDR-64–72, Air Force Weapons Laboratory, Cambridge, MA.
Tse, S.T. & Rice, J.R., 1986. Crustal earthquake instability in relation to the depth variation of frictional slip properties, *J. geophys. Res.,* **91,** 9452–9472.
Umeda, Y., 1992. The bright spot of an earthquake, *Tectonophysics,* **211,** 13–22.
Zheng, G. & Rice, J.R., 1998. Conditions under which velocity-weakening friction allows a self-healing versus a cracklike mode of rupture, *Bull. seism. Soc. Am.,* **88,** 1466–1483.

APPENDIX A: RELATION BETWEEN THE SW CHARACTERISTIC LENGTH AND THE BREAKDOWN TIME

In this Appendix we derive an expression that connects the SW characteristic distance d_0 and the breakdown time T_b. Let us consider an arbitrary point on the x_1–t plane of the crack tip (x_1^*, t^*); by definition, the slip at this point is zero: $u(x_1^*, t^*)=0$. Let us consider also the point (x_1^*, t^*+T_b); by definition of the breakdown time, $u(x_1^*, t^*+T_b)=d_0$. Therefore, we have

$$\frac{u(x_1^*, t^*+T_b)-u(x_1^*, t^*)}{T_b}=\frac{d_0}{T_b}\,. \tag{A1}$$

In general, the breakdown time is a whole multiple of the time step,

$$T_b=n\Delta t\,, \qquad n\geq 1\,,$$

and thus it is possible to write eq. (A1) as follows:

$$\begin{aligned}\frac{u(x_1^*, t^*+T_b)-u(x_1^*, t^*)}{n\Delta t}&=\frac{1}{n\Delta t}\,[u(x_1^*, t^*+T_b)-u(x_1^*, t^*+T_b-\Delta t)\\&\quad+u(x_1^*, t^*+T_b-\Delta t)+\ldots\\&\quad-u(x_1^*, t^*+T_b-(n-1)\Delta t\\&\quad+u(x_1^*, t^*+T_b-(n-1)\Delta t)-u(x_1^*, t^*)]\,.\end{aligned} \tag{A2}$$

In eq. (A2) we have added and subtracted pairs of values of displacement u in the time steps between $t^*+T_b-\Delta t$ and $t^*+T_b-(n-1)\Delta t$. In this way, in eq. (A2) we recognize the definition of the slip velocity, and therefore we rewrite eq. (A2) as

$$\frac{1}{n}\sum_{k=1}^{n}\dot{u}(x_1^*, t^*+T_b-(k-1)\Delta t)\,. \tag{A3}$$

Inserting eq. (A3) into eq. (A1) we have

$$d_0 = T_b(x_1^*) \frac{\sum_{k=1}^{n} \dot{u}(x_1^*, t^* + T_b - (k-1)\Delta t)}{n} . \quad (A4)$$

In this expression we have indicated the dependence of T_b on x_1^* to emphasize the fact that the breakdown time is variable along the fault line, as discussed in Section 4.1. If we denote with the symbol $< \ldots >_{T_b}$ the average of the slip velocity over the times t_b within the cohesive zone (where the displacement is between 0 and d_0), we can rewrite formula (A4) for d_0 as

$$d_0 = T_b(x_1^*) \langle \dot{u}(x_1^*, t_b) \rangle_{T_b} . \quad (A5)$$

This relation is equivalent to eq. (2) of Guatteri & Spudich (2000). According to Ohnaka & Yamashita (1989) (their eq. 59), we have

$$\langle \dot{u} \rangle_{Tb} = \frac{v_{crack}}{C(v_{crack})} \frac{\tau_u}{\mu} , \quad (A6)$$

where μ is the rigidity, v_{crack} is the rupture velocity and $C(v_{crack})$ is a function of rupture velocity defined by the authors.

APPENDIX B: DEFINITION OF THE MISFIT FUNCTION

In order to quantify in a rigorous way the differences existing between the solutions obtained by using the BIE and the FD approach, we have introduced in the x_1–t plane the adimensional misfit function $m(x_i, t_n)$, defined as

$$m(x_i, t_n) = \frac{|u^{(BIE)}(x_i, t_n) - \tilde{u}^{(FD)}(x_i, t_n)|}{u^{(BIE)}(x_i, t_n) - \tilde{u}^{(FD)}(x_i, t_n)} . \quad (B1)$$

In eq. (B1) $u^{(BIE)}$ denotes the slip obtained with the BIE method, while $\tilde{u}^{(FD)}$ is the value of the slip arising from the FD approach. While the solutions of the dynamic problem are defined at the same position along the x_1-coordinate, along the t-coordinate they are defined at different points, because $t_n = (n-1)\Delta t$ and $\Delta t^{(BIE)} \neq \Delta t^{(FD)}$. We have therefore resampled the values of the array $u^{(FD)}(x_i, t_n^{(FD)})$ into the array $\tilde{u}^{(FD)}(x_i, t_n^{(BIE)})$ by means of a linear interpolation in time. Eq. (B1) has been used in a similar form by Nostro *et al.* (1999); the misfit m is the range [0, 1].

APPENDIX C: STABILITY AND RESOLUTION OF THE SOLUTIONS

C1 The slip-weakening law

C1.1 The boundary integral equation method

In order to obtain physically acceptable solutions by using the BIE method, several conditions have to be satisfied to determine a correct discretization of the dynamic problem. We recall that eq. (2.4) is valid under the assumption that $\Delta x \geq v_P \Delta t$. This condition is typical of all the boundary integral equation methods. According to Andrews (1985), the solution of the numerical procedure is unique if the following condition is satisfied:

$$\Delta x < -\frac{\mu v_P}{v_S \frac{d}{du} \tau} ,$$

or for the in-plane crack geometry examined in this study,

$$\frac{l_c^{(II)}}{\Delta x} > \frac{2}{\pi} \frac{a-1}{a\sqrt{a}} (1+S)^2 ,$$

where a is the square root of the v_P/v_S ratio ($a^2 \equiv v_P/v_S$), S is the strength parameter previously defined and $l_c^{(II)}$ is the critical halfplane (mode II) geometry (see Appendix D).

In order to resolve the cohesive zone (that is, to verify that the discretization guarantees a sufficient number of points in the breakdown zone, Fig. 5) it is required that $\Delta x < X_b$ (where X_b is the spatial extension of the cohesive zone) or, equivalently, that $\Delta t < T_b$. From eq. (A1) we can write

$$\Delta t < \frac{d_0}{\langle \dot{u}(x_1^*, t_b) \rangle_{T_b}} ,$$

or, taking into account that $\Delta t = w \Delta x / v_S$,

$$\Delta x < \frac{v_S}{w} \frac{1}{\langle \dot{u}(x_1^*, t_b) \rangle_{T_b}} d_0 = \frac{v_S}{w} \frac{C(v_{crack})}{v_{crack}} \frac{\mu}{\tau_u} d_0 .$$

In order to satisfy this condition, it is a reasonable assumption to consider $\Delta x \ll d_0$. This condition is more suitable for numerical purposes since the dimension of X_b changes during the rupture propagation. In our study we have shown that a very suitable choice is $d_0 > 7\Delta x$.

We emphasize that these conditions are quite important for verifying the dynamic solutions. In particular, the last condition is very important in order to take into account the adopted constitutive law properly.

C1.2 The finite difference method

Unlike BIE methods, the FD approach does not require particular constraints on Δx and Δt. The only necessary condition is the resolution of the breakdown zone, as discussed above. In all the simulations presented and discussed in this study, the stability conditions are satisfied. We point out that, even if some of the previous conditions are not verified, the slip behaviour might still be acceptable; however, the traction and the slip velocity show complex time histories and the phase diagrams reveal an artificial complexity that is due to the numerical solution.

C2 The Dieterich–Ruina laws

By studying the the dynamic problem in the quasi-static approximation, Rice (1993) has shown that, if the spatial step in the numerical simulation is greater than a fixed critical value h^*, artificial complexity is introduced into the solutions. This result has been confirmed in the dynamic regime by Rice & Ben-Zion (1996). The quantity h^* is expressed as (Rice 1993)

$$h^* = \frac{2\mu L}{\pi [(b-a)\sigma_n^{eff}]_{max}} ,$$

where $[(b-a)\sigma_n^{eff}]_{max}$ is the combination of the constitutive parameters A and B maximizing on the fault surface the function

$$\chi(B-A) = -v \frac{d}{dv} \tau^{ss}(v) .$$

Because for the Dieterich–Ruina law χ is a monotonic function of the variable $(B-A)$, the greatest value of $(B-A)$ on the fault provides its maximum. Therefore, Rice's condition

can be expressed as

$$\Delta x \ll \frac{2\mu L}{\pi[(b-a)\sigma_n^{\rm eff}]_{\rm max\ on\ the\ fault}}\,.$$

The quanity h^* has the physical meaning of the minimum extension of the nucleation zone; for both the RD and the DR laws in the quasi-static approximation, h^* is

$$h^* = \frac{2l_c}{\eta\pi}$$

where η is a factor depending by the fault geometry (see Section 5.1). As shown in the aforementioned papers, this stability condition avoids artificial complexity in the numerical solutions.

APPENDIX D: CORRESPONDENCE BETWEEN THE FRACTURE ENERGY AND THE CRITICAL LENGTH IN DIFFERNT CONSTITUTIVE EQUATIONS

In Section 5.1 we derived the relations between the constitutive parameters of the DR and those of the SW governing equations. Here we propose a correspondence between the fracture energy G and the critical half-length l_c and we compare the definitions of l_c in the frameworks of this two constitutive laws.

In general, the fracture energy G can be expressed as (Ida 1972; Aki 1979)

$$G = \frac{1}{2}\int_0^{+\infty} (\tau(u) - \tau_f)du\,. \tag{D1}$$

In the SW friction model of Fig. 1(a) this relation gives

$$G^{(\rm SW)} = (\tau_u - \tau_f)\,\frac{d_0}{4}\,, \tag{D2}$$

whereas for the rate- and state-dependent friction laws (using the approximate expression for the friction) it gives

$$G^{(\rm DR)} = \frac{1}{4}\left[\tau^{\rm ss}(v_{\rm init}) + a\sigma_n^{\rm eff}\ln\left(\frac{v_2}{v_{\rm init}}\right) - \tau^{\rm ss}(v_2)\right]L\,. \tag{D3}$$

We emphasize that with both the SW and the DR laws the energy released in the rupture process increases linearly with the characteristic length and with the difference between the peak value reached by the friction and the final kinetic level.

In both models a minimum extension exists, also called the critical patch size, below which a crack cannot propagate. Andrews (1976b), starting from considerations based on energy balance principles for planar shear fractures, found that for mode II (in-plane) cracks propagation is possible only when the rupture has a half-length greater then a threshold value, whose expression gives

$$l_c^{(\rm II)} = 2\,\frac{\mu}{\pi}\,\frac{\lambda+\mu}{\lambda+2\mu}\,\frac{\tau_u - \tau_f}{(\tau_0 - \tau_f)^2}\,d_0\,. \tag{D4}$$

An equivalent expression has been introduced for the rate- and state-dependent friction laws. Studies performed on the stability of spring-slider systems with only one degree of freedom (e.g. Dieterich 1986 and references therein; Rice & Ruina 1983; Gu *et al.* 1984) have shown that the slip can accelerate to the instability if the stiffness k of the mass spring system is less than a critical value, expressed by the relation

$$k_{\rm cr} = \kappa\,\frac{\sigma_n^{\rm eff}}{L}\,, \tag{D5}$$

where κ is a constant depending on the parameters of the adopted constitutive law and on the conditions under which the experiment is performed. In particular, in the quasi-static approximations [for both the RD law (Gu *et al.* 1984) and the DR governing equation (Ranjith & Rice 1999)] the result is $\kappa = b - a$. Combining the results for a spring-slider system with the solutions for the displacement due to a crack in an elastic medium, assuming that the properties and the conditions in the centre of the crack are adequate to represent of the entire rupture, we obtain (Dieterich 1986, 1992)

$$k = \mu\,\frac{\eta}{l}\,, \tag{D6}$$

where η is a factor depending on the rupture geometry (Dieterich 1992) and l is the half-length—or the radius—of the crack.

Comparings eqs (D5) and (D6), it is possible to write an approximate relation for the minimum half-length, which gives an unstable behaviour,

$$l_c = \eta\mu\,\frac{L}{\kappa\sigma_n^{\rm eff}}\,. \tag{D7}$$